Chapter 3

Governing differential equations for natural circulation systems

3.1 Introduction

Before using a natural circulation loop for a particular application, often it is required to estimate its heat transport capability. In many instances, natural circulation loops have to be started up from a stagnant initial condition or may be subject to transients due to change in heat source and heat sink conditions. In addition, natural circulation loops are susceptible to instability of various types. Thus, it is necessary to estimate the steady-state, transient, and stability performance of the natural circulation loop under consideration. A prerequisite for the analysis of industrial natural circulation systems (NCSs) is to arrive at the governing differential equations representing the conservation of mass, momentum, and energy. Generally, a one-dimensional approach is followed in the analysis of NCSs. The one-dimensional analysis also requires constitutive relationships for friction and heat transfer depending on the state of the fluid. An equation of state for the working fluid in the natural circulation loop is also required for closure. The intention of this chapter is to derive the equations governing NCSs from first principles and to present the constitutive relationships commonly used in natural circulation analysis. Additionally, it provides some details and references for the equation of state for the fluids of common interest to advanced reactor systems.

3.2 General differential equations for natural circulation systems

A thermo-fluid-dynamical system like the natural circulation loop must obey the laws of conservation of mass, momentum, and energy. Consider a simple uniform-diameter rectangular loop as shown in Fig. 3.1 with a heater and a cooler connected by insulated pipes. The outer surface of the heater is supplied with a uniform heat flux of q'' and the tube-in-tube-type cooler is supplied with a coolant at a mass flow rate of w_s at constant temperature T_s. Since the NCS is essentially a pipe loop, one-dimensional formulation is assumed to be valid for design and analysis. In one-dimensional formulation, the only coordinate "s" runs around the loop with its origin at the beginning

Single-phase, Two-phase and Supercritical Natural Circulation Systems.
DOI: https://doi.org/10.1016/B978-0-08-102486-7.00003-2

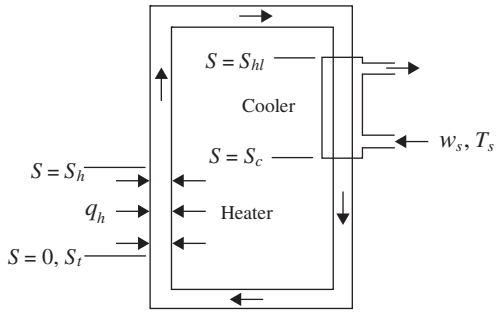

FIGURE 3.1 Single-phase natural circulation loop.

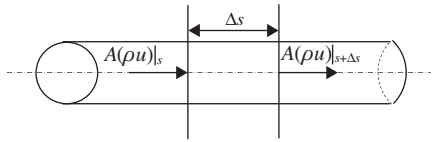

FIGURE 3.2 Conservation of mass.

of the heater section as shown in Fig. 3.1. Consider a small segment of the pipe of length Δs (see Fig. 3.2) with flow area of "A" containing a fluid of density ρ.

The law of conservation of mass for the pipe segment of length Δs in Fig. 3.2 can be stated as

$$\begin{pmatrix}\text{Mass flow rate}\\ \text{entering segment } \Delta s\end{pmatrix} - \begin{pmatrix}\text{Mass flow rate}\\ \text{leaving segment } \Delta s\end{pmatrix} = \begin{pmatrix}\text{Rate of mass accumulation}\\ \text{in the segment } \Delta s\end{pmatrix} \tag{3.1}$$

Mathematically it can be written as

$$(A\rho u)|_s - (A\rho u)\big|_{s+\Delta s} = A\Delta s\frac{\partial \rho}{\partial t} \tag{3.2}$$

where A is the flow area of the uniform-diameter pipe, t is the time, ρ and u are, respectively, the density and the velocity of the fluid. Dividing throughout by $A\Delta s$ and rearranging one obtains

$$\frac{\partial \rho}{\partial t} + \frac{\partial(\rho u)}{\partial s} = 0 \tag{3.3}$$

Similarly, the momentum conservation is essentially Newton's 2nd law of motion which can be stated for the pipe segment Δs shown in Fig. 3.3 as

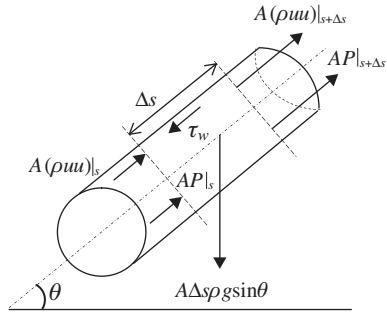

FIGURE 3.3 Conservation of momentum.

$$\begin{pmatrix}\text{Rate of change of momentum of}\\ \text{fluid inside the pipe segment } \Delta s\end{pmatrix} = \begin{pmatrix}\text{Momentum in} -\\ \text{Momentum out}\end{pmatrix} + \begin{pmatrix}\text{Sum of applied forces on the}\\ \text{fluid inside the pipe segment } \Delta s\end{pmatrix} \tag{3.4}$$

Mathematically this can be written as (see Fig. 3.3)

$$A(\rho uu)|_s - A(\rho uu)|_{s+\Delta s} + AP|_s - AP|_{s+\Delta s} - \tau_w \xi \Delta s - A\Delta s\rho g\ \sin\theta = A\Delta s\frac{\partial(\rho u)}{\partial t} \tag{3.5}$$

Dividing throughout by $A\Delta s$ and rearranging we get

$$\frac{\partial(\rho u)}{\partial t} + \frac{\partial(\rho uu)}{\partial s} + \frac{\partial P}{\partial s} + \frac{\tau_w \xi}{A} + \rho g \sin\theta = 0 \tag{3.6}$$

where θ is the angle that the flow direction makes with the horizontal and ξ is the wetted perimeter of the pipe. Noting that $\tau_w = f\rho u^2/8$ (where f is the Darcy−Weisbach friction coefficient) and $\xi/A = 4/D$, we get

$$\frac{\partial(pu)}{\partial t} + \frac{\partial(puu)}{\partial s} + \frac{\partial P}{\partial s} + \frac{fpu^2}{2D} + pg \sin\theta = 0 \tag{3.7}$$

Note that every term in the above equation has the units of pressure drop per unit length. The first term denotes pressure drop due to the inertia, the second term signifies the acceleration pressure drop, the third term the static pressure drop, the fourth term the frictional pressure drop, and the last term the gravitational or elevation pressure drop.

Neglecting viscous dissipation and pressure work, the energy conservation for a segment in the heater (see Fig. 3.4) can be written as

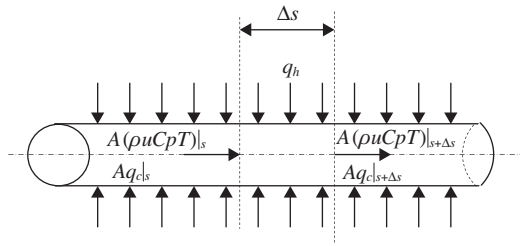

FIGURE 3.4 Conservation of energy.

$$\begin{pmatrix}\text{Net rate of heat transfer by}\\ \text{convection and conduction to}\\ \text{the fluid in the pipe segment } \Delta s\end{pmatrix} + \begin{pmatrix}\text{Rate of heat transfer}\\ \text{from the wall to the}\\ \text{fluid in the segment } \Delta s\end{pmatrix} = \begin{pmatrix}\text{Rate of accumulation}\\ \text{of heat in the fluid}\\ \text{segment } \Delta s\end{pmatrix} \tag{3.8}$$

$$A(\rho uCpT)|_s - A(\rho uCpT)|_{s+\Delta s} + Aq_c|_s - Aq_c|_{s+\Delta s} + \xi \Delta s q_h = A\Delta s \frac{\partial(\rho CpT)}{\partial t} \tag{3.9}$$

Dividing throughout by $A\Delta s$ and rearranging, we obtain

$$\frac{\partial(\rho CpT)}{\partial t} + \frac{\partial(\rho uCpT)}{\partial s} + \frac{\partial q_c}{\partial s} = \frac{\xi q_h}{A} \tag{3.10}$$

The heat flux due to conduction can be expressed as

$$q_c = -k\frac{\partial T}{\partial s} \tag{3.11}$$

Using Eq. (3.11) in Eq. (3.10) and noting that $\xi/A = 4/D$ for a circular pipe, we obtain,

$$\frac{\partial(\rho CpT)}{\partial t} + \frac{\partial(\rho uCpT)}{\partial s} + \frac{\partial}{\partial s}\left(-k\frac{\partial T}{\partial s}\right) = \frac{4q_h}{D} \tag{3.12}$$

Following a similar procedure, equations can be obtained for the insulated pipes and the cooler so that the complete energy equation for the natural circulation loop can be written as

$$\frac{\partial(\rho CpT)}{\partial t}+\frac{\partial(\rho uCpT)}{\partial s}+\frac{\partial}{\partial s}\left(-k\frac{\partial T}{\partial s}\right)=\begin{cases}\dfrac{4q_h}{D} & \text{heater} \quad (\text{for} \quad 0<s\le s_h)\\ 0 & \text{pipes} \quad (\text{for} \quad s_h<s\le s_{hl} \quad \text{and} \quad s_c<s\le S_t)\\ -\dfrac{4U_i}{D}(T-T_s) & \text{cooler} \quad (\text{for} \quad s_{hl}<s\le s_c)\end{cases} \tag{3.13}$$

where U_i is the overall heat transfer coefficient based on the inside heat transfer area of the cooler.

3.3 Special cases

Natural circulation loops can be closed or open. As already mentioned in Chapter 1 an open loop is one which exchanges both energy and mass with the surroundings, whereas a closed loop exchanges only energy with the surroundings. All the natural circulation-based steam-generating systems, such as the steam generator in pressurized-water reactors (PWRs), pressurized heavy-water reactors (PHWRs) and Russian VVERs, the NC-based boiling water reactors (NCBWRs), the natural circulation boilers in fossil-fired power plants and the thermosyphon reboiler in distillation columns are all examples of open-loop NCSs. On the other hand, primary heat transport system of most PWRs, PHWRs and VVERs operates in the closed-loop mode during pumping power failures and station blackouts (SBOs). In addition, the NCSs can be single-phase, two-phase, or supercritical, depending on the state of the working fluid. Since analytical treatments for open and closed loops are different depending on the state of the fluid, it is appropriate to consider these special cases.

3.3.1 Closed-loop single-phase natural circulation systems

Fig. 3.1 represents the geometry and coordinate system used for the single-phase NCS under consideration. In general, single-phase liquids are considered incompressible, and therefore the mass conservation equation can be rewritten as

$$\frac{\partial u}{\partial s}=0 \tag{3.14}$$

The above equation implies that the velocity is independent of position in a uniform-diameter loop and is only a function of time. Often, it is convenient to work with the integral momentum equation. The integral momentum equation can be obtained by integrating Eq. (3.7) over a closed loop to yield the following equation:

$$L_t \rho \frac{du}{dt} + \frac{f L_t \rho u^2}{2D} + g \oint \rho dz = 0 \tag{3.15}$$

Note that $ds \sin\theta = dz$ has been used in the above equation. As the sum of the pressure drop over a closed loop is zero, the pressure term vanishes from the momentum equation, which is the main advantage of the integral momentum equation as would be seen later while numerically solving it. Furthermore, the sum of the acceleration pressure drop also becomes zero over the closed loop. Additionally, if Boussinesq approximation is valid, then the fluid properties are assumed constant except for the density in the buoyancy force term which can be expressed as

$$\rho = \rho_0 \left[1 - \beta_T (T - T_0)\right] \tag{3.16a}$$

where

$$\beta_T = \frac{1}{v} \left(\frac{\partial v}{\partial T} \right)_p \tag{3.16b}$$

Note that ρ_0 is a reference density at the reference temperature T_0. It may be mentioned that the Boussinesq approximation is valid for only small temperature differences. Use of Boussinesq approximation was found to give a good match with test data for temperature differences between the hot and cold legs as high as 30°C if the loop average temperature was used as the reference value. Using this, Eq. (3.15) becomes

$$L_t \rho_0 \frac{du}{dt} + \frac{f L_t \rho_0 u^2}{2D} - \rho_0 \beta_T g \oint T dz = 0 \tag{3.17}$$

Note that Eq. (3.17) is an ordinary differential equation. Often, the friction coefficient can be expressed as

$$f = p / Re^b \tag{3.18}$$

Using this, the momentum equation can be rewritten as

$$L_t \rho_0 \frac{du}{dt} + \frac{p L_t \rho_0^{1-b} \mu^b u^{2-b}}{2D^{1+b}} - \rho_0 \beta_T g \oint T dz = 0 \tag{3.19}$$

For constant fluid properties, Eq. (3.13) can be rewritten as

$$\frac{\partial T}{\partial t}+u\frac{\partial T}{\partial s}-\alpha_d\frac{\partial^2 T}{\partial s^2}=\left\{\begin{array}{lll}\dfrac{4q_h}{D\rho_0 Cp} & \text{heater} & \text{for } 0<s\le s_h\\ 0 & \text{pipes} & \text{for } s_h<s\le s_{hl} \text{ and } s_c<s\le s_t\\ \dfrac{-4U_i}{D\rho_0 Cp} & \text{cooler} & \text{for } s_{hl}<s\le s_c\end{array}\right\} \tag{3.20}$$

Note that the fluid properties in the hot leg, cold leg, the source and the sink are all different. Hence it is important to select an appropriate reference temperature to calculate the reference density. Since the friction pressure drop occurs over the entire loop as well as the driving buoyancy pressure differential depends on the temperature integral over the entire loop, it is appropriate to use the loop average temperature as the reference value to calculate the fluid properties.

Since the heat transport capability of natural circulation loops is directly proportional to the generated mass flow rate, w, often the governing equations are expressed in terms of the mass flow rate. Therefore the conservation equations of mass, momentum, and energy can be rewritten as

$$\frac{\partial w}{\partial s}=0 \tag{3.21}$$

$$\frac{L_t}{A}\frac{dw}{dt}+\frac{pL_t\mu^b w^{2-b}}{2D^{1+b}\rho_0 A^{2-b}}-\rho_0\beta_T g\oint Tdz=0 \tag{3.22}$$

$$\frac{\partial T}{\partial t}+\frac{w}{A\rho_0}\frac{\partial T}{\partial s}-\alpha_d\frac{\partial^2 T}{\partial s^2}=\left\{\begin{array}{lll}\dfrac{4q_h}{D\rho_0 Cp} & \text{heater} & \text{for } 0<s\le s_h\\ 0 & \text{pipes} & \text{for } s_h<s\le s_{hl} \text{ and } s_c<s\le s_t\\ -\dfrac{4U_i(T-T_s)}{D\rho_0 Cp} & \text{cooler} & \text{for } s_{hl}<s\le s_c\end{array}\right\} \tag{3.23}$$

For ordinary fluids like water, the axial conduction term can be neglected from Eqs. (3.20) and (3.23). In addition, the pipes are considered to be adiabatic in the above derivation. Often, some natural convective heat losses are unavoidable through the insulated pipes. Accounting for this, the energy equation can be rewritten as

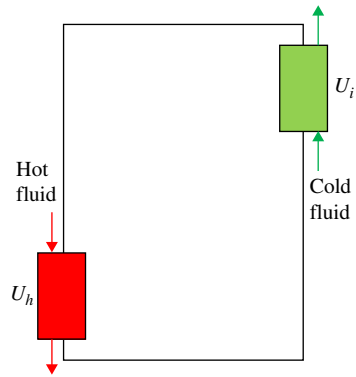

FIGURE 3.5 NCL with source and sink formed by HXs.

$$\frac{\partial T}{\partial t}+\frac{w}{A\rho_0}\frac{\partial T}{\partial s}=\left\{\begin{array}{lll}\dfrac{4q_h}{D\rho_0 Cp} & \text{heater} & \text{for } 0<s\le s_h\\ -\dfrac{4U_a}{D\rho_0 Cp} & \text{pipes} & \text{for } s_h<s\le s_{hl} \text{ and } s_c<s\le s_t\\ -\dfrac{4U_i(T-T_s)}{D\rho_0 Cp} & \text{cooler} & \text{for } s_{hl}<s\le s_c\end{array}\right\} \tag{3.24}$$

where U_a is the overall heat transfer coefficient to account for the ambient heat losses through the insulated pipe. If the closed loop NCS is formed by two heat exchangers (HXs), then the energy equation is modified as (see also Fig. 3.5),

$$\frac{\partial T}{\partial t}+\frac{w}{A\rho_0}\frac{\partial T}{\partial s}=\left\{\begin{array}{ll}\dfrac{4U_h(T-T_h)}{D\rho_0 Cp} & \text{heater for } 0<s\le s_h\\ -\dfrac{4U_a(T-T_a)}{D\rho_0 Cp} & \text{pipes for } s_h<s\le s_{hl} \text{ and } s_c<s\le s_t\\ -\dfrac{4U_i(T-T_c)}{D\rho_0 Cp} & \text{cooler for } s_{hl}<s\le s_c\end{array}\right\} \tag{3.25}$$

where U_h is the overall heat transfer coefficient based on the inside heat transfer area of the heater.

3.3.2 Open-loop single-phase natural circulation

Often the last heat transport system in a coupled NCS is an open system. Many closed-loop NCSs reject the heat to the ultimate heat sink through an

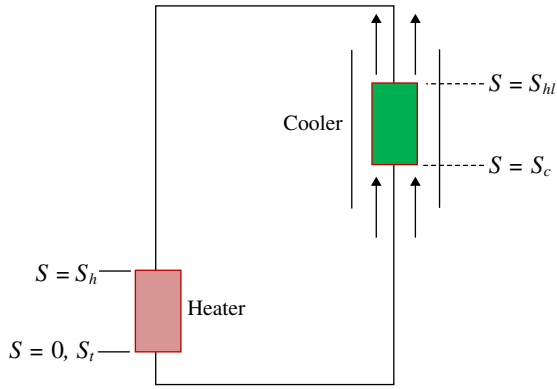

FIGURE 3.6 Combination of single-phase closed-loop natural circulation with an open-loop NCS.

open-loop NCS. Such systems are employed in the nuclear industry to extend passive operation of heat transport systems indefinitely. Besides nuclear, such systems are of interest to solar thermal power plants. A closed-loop NCS in combination with an open-loop NCS makes it completely passive, enabling its operation during a station blackout (i.e., complete loss of AC power). The simplest example of such a combination of an open-loop and closed-loop NCS is shown in Fig. 3.6. As can be seen from Fig. 3.6, a simple hollow pipe around the cooler of the closed-loop NCS makes the simplest open-loop NCS. Such simple systems are possible if the heat sink is immersed in a fluid. However, indefinite operation is possible only if the heat sink is immersed in the atmosphere or the ocean.

Unlike a closed-loop NCS, the essential hardware of an open-loop NCS is just a heat source. The heat source may or may not have unheated pipe sections connected to it. For the purpose of the analysis, consider the open-loop NCS shown in Fig. 3.7 with a heated length of L_h and unheated lengths of L_i and L_o at the inlet and outlet of the heated section, respectively. The unheated lengths are insulated and the heat flux is specified. In addition, the inlet temperature T_i and fluid density at the inlet ρ_i are specified.

The conservation equation of mass remains the same as that given in Eq. (3.21). For the momentum Eq. (3.7) must now be integrated over the inlet and outlet of the open-loop NCS assuming fluid properties to be constant except density in the buoyancy force term. Integrating and rearranging it in terms of the mass flow rate, one obtains

$$\frac{L_t}{A}\frac{dw}{dt} + \frac{1}{A^2}\int_{s=0}^{L_t} d\left(w^2 v\right) + \frac{pL_t\mu^b w^{2-b}}{2D^{1+b}\rho_0 A^{2-b}} + P_o - P_i - g\int_{s=0}^{s=L_t}\rho dz = 0 \quad (3.26)$$

where v is the specific volume and the second term on the LHS denotes the acceleration pressure drop which does not become zero for an open loop.

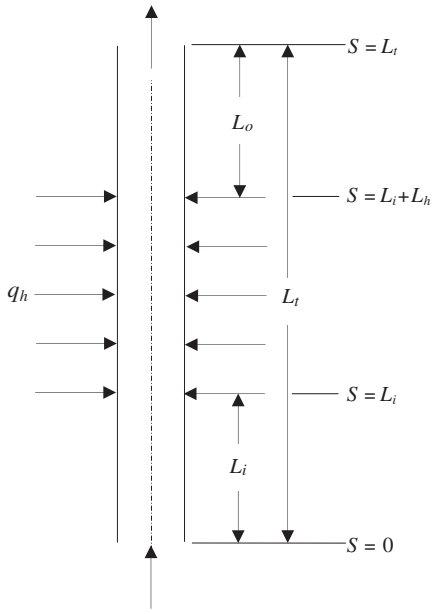

FIGURE 3.7 Simple open-loop NCS considered for analysis.

Note that the difference between the inlet and the outlet pressures is essentially due to the column of fluid. Therefore

$$P_i = P_o + \rho_i g L_t \tag{3.27}$$

Using this, the integral momentum equation becomes

$$\frac{L_t}{A}\frac{dw}{dt} + \frac{1}{A^2}\int_{s=0}^{L_t} d\left(w^2 v\right) + \frac{pL_t \mu^b w^{2-b}}{2D^{1+b}\rho_0 A^{2-b}} - \rho_i g L_t - g\int_{s=0}^{s=L_t} \rho dz = 0 \tag{3.28}$$

Note that the pressure term is again vanishing from the integral momentum equation. In this derivation, the local pressure losses were assumed negligible. The energy equation for the open loop can be written as

$$\frac{\partial T}{\partial t} + \frac{w}{A\rho_0}\frac{\partial T}{\partial s} = \left\{ \begin{array}{ll} \dfrac{4q_h}{D\rho_0 Cp} & \text{heater for } L_i < s \le L_i + L_h \\ 0 & \text{pipes for } 0 < s \le L_i \text{ and } L_i + L_h < s \le L_t \end{array} \right\} \tag{3.29}$$

Generally, to enhance the flow rate often a tall riser (i.e., the height above the heated section, L_o in this case) is employed.

Problem 1: Consider the two open-loop NCSs shown in Fig. 3.8. Neglecting local pressure losses identify which of them generates higher mass flow rate

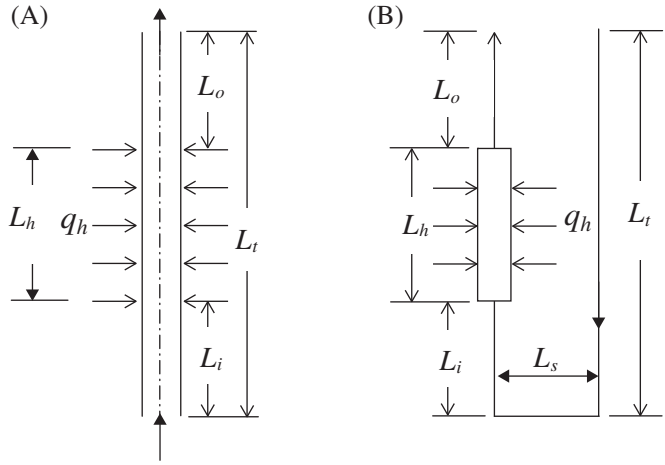

FIGURE 3.8 Simple open-loop NCS considered for analysis: (A) open vertical loop; (B) open U-loop.

if the heated length L_h, inlet conditions (i.e., T_i and ρ_i), and heat flux q_h are the same in both systems?

3.3.3 Closed-loop two-phase natural circulation systems

Analysis of two-phase flow is rather complex with several flow patterns starting from subcooled single-phase flow to bubbly flow, slug flow, churn flow, annular flow, droplet flow, and finally to single-phase vapor flow. The flow patterns also depend on the orientation (i.e., vertical upward, downward, inclined, or horizontal) of the flow path. Thermodynamic and hydrodynamic nonequilibrium can exist, which further complicates the analysis. Several two-phase flow models are in common use starting from the homogeneous equilibrium model (HEM) which does not account for the difference in velocity and temperature between the vapor and liquid phases. The simplest model that can account for the difference in velocities is the drift flux model (DFM). The present-day thermal hydraulic system codes generally employ the two-fluid model (TFM) which is able to account for both unequal velocity and unequal temperature between the liquid and the vapor phases. The TFM involves six equations with three equations for each phase to represent the mass, momentum and energy conservation. Also, the TFM with a single area-averaged pressure is known to be mathematically ill-posed. This means that if we perform a linear stability analysis of the TFM equations with single pressure, then it will be always unstable. However, Zhou and Podowski (2001) as well as Song and Ishii (2001) have reported novel approaches for the stability analysis of the two-fluid equations. Considering the complexity of the analysis using the two-fluid and the DFMs, in this book we deal with only HEM.

Commonly used one-dimensional conservation equations applicable to two-phase NCSs based on the HEM are presented in this section. A closed-loop two-phase NCS considered for analysis is shown in Fig. 3.9. The pipes are considered to be adiabatic. The heater is assumed to be supplied with a uniform heat flux and the cooler secondary side is assumed to be at constant temperature, T_s.

For the two-phase NCS, the governing mass conservation equation is the same as Eq. (3.3). The momentum conservation equation is also given by Eq. (3.7). In two-phase systems, because of phase change, one often prefers to work with enthalpy as it is a continuous function, unlike temperature which is discontinuous. Hence the temperature is replaced by enthalpy assuming Cp is a constant in the energy Eq. (3.13) resulting in the following equation

$$\frac{\partial(\rho i)}{\partial t}+\frac{\partial(\rho u i)}{\partial s}=\left\{\begin{array}{ll}\dfrac{4q_h}{D} & \text{heater for } 0<s\le L_h\\ 0 & \text{pipes for } L_h<s\le L_{hl} \text{ and } L_c<s\le L_t\\ -\dfrac{4U_i(T-T_s)}{D} & \text{cooler for } L_{hl}<s\le L_c\end{array}\right\} \tag{3.30}$$

Note that the axial conduction has been neglected in Eq. (3.30), which is appropriate for ordinary fluids. If the pressure drop in the loop is negligible compared to the hydrostatic pressure of the loop, then the fluid properties can be considered constant. We can also express density by a Boussinesq-type relation in terms of the enthalpy as

$$\rho=\rho_0\left[1-\beta_h(i-i_0)\right] \tag{3.31}$$

where

$$\beta_h=\frac{1}{\bar{v}}\left(\frac{\partial v}{\partial i}\right)_P \tag{3.32}$$

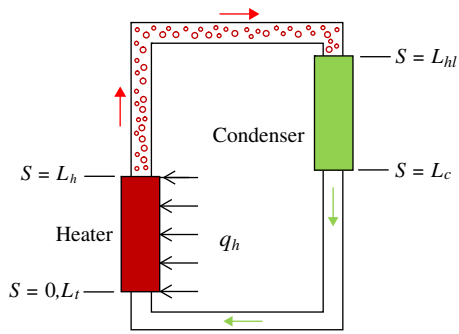

FIGURE 3.9 Closed-loop two-phase NCS considered for analysis.

Using Eq. (3.31) in the density integral of the momentum equation, we get

$$L_t \frac{\partial(\rho u)}{\partial t} + \oint \partial(\rho u u) + \frac{f L_t \rho u^2}{2D} + g\rho_0 \beta_h \oint i \partial z = 0 \tag{3.33}$$

Thus, the energy and momentum equations for two-phase NCS become similar to that of single-phase NCS. Expressing in terms of the mass flow rate, the mass, momentum, and energy equations become

$$\frac{\partial \rho}{\partial t} + \frac{1}{A}\frac{\partial w}{\partial s} = 0 \tag{3.34}$$

$$\frac{L_t}{A}\frac{\partial w}{\partial t} + \frac{1}{A^2}\oint \partial\left(w^2 v\right) + \frac{f L_t w^2}{2D\rho A^2} + g\rho_0 \beta_h \oint i \partial z = 0 \tag{3.35}$$

$$\frac{\partial(\rho i)}{\partial t} + \frac{1}{A}\frac{\partial(wi)}{\partial s} = \begin{Bmatrix} \dfrac{4q_h}{D} & \text{heater for } 0 < s \le L_h \\ 0 & \text{pipes for } L_h < s \le L_{hl} \text{ and } L_c < s \le L_t \\ -\dfrac{4U_i(T - T_s)}{D} & \text{cooler for } L_{hl} < s \le L_c \end{Bmatrix} \tag{3.36}$$

For homogeneous two-phase flow, the density can be expressed as

$$\rho = \alpha\rho_g + (1 - \alpha)\rho_f \tag{3.37}$$

where the void fraction α for two-phase flow is given by

$$\alpha = \frac{1}{1 + \frac{(1-x)}{x}\frac{\rho_g}{\rho_f}\frac{u_g}{u_f}} = \frac{1}{1 + \frac{(1-x)}{x}\frac{\rho_g S}{\rho_f}} \tag{3.38}$$

For homogeneous equilibrium flow, $u_g = u_f$ leading to slip ratio $S = 1$ and hence the void fraction is given by

$$\alpha = \frac{1}{1 + \frac{(1-x)}{x}\frac{\rho_g}{\rho_f}} \tag{3.39}$$

Since $v = xv_g + (1 - x)v_f = v_f + xv_{fg}$ and $i = xi_g + (1 - x)i_f = xi_{fg} + i_f$ for homogeneous two-phase flow with $v_{fg} = v_g - v_f$ and $i_{fg} = i_g - i_f$ we obtain

$$\left(\frac{\partial v}{\partial i}\right)_P = \frac{v_{fg}}{i_{fg}};\ \text{so that } \beta_h = \frac{1}{xv_{fg} + v_f}\frac{v_{fg}}{i_{fg}} \tag{3.40}$$

Using this in Eq. (3.31), the density can be calculated. This is compared with the density calculated by using Eq. (3.37) in Fig. 3.10. As can be seen from the figure, the density calculated by both equations is identical.

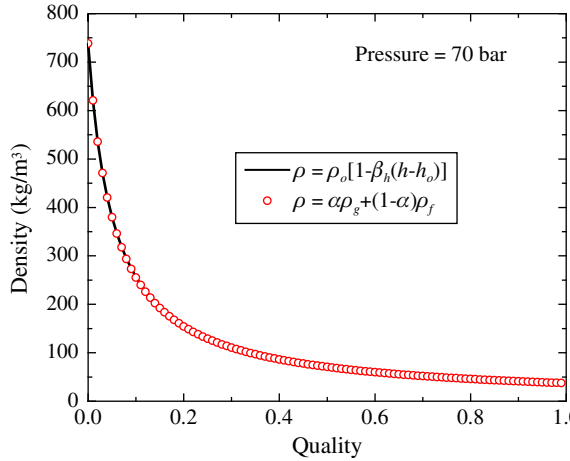

FIGURE 3.10 Density predicted by Eqs. (3.31) and (3.37).

The same approach is also reported in Gartia et al. (2006). Since this is a kind of Boussinesq approximation for two-phase flow, the variation of β_h for different fluids need to be examined in detail to check its validity. Gartia et al. (2006) also examined its applicability for water and found that a constant value of β_h is valid in the high-pressure region for small changes in quality. In Fig. 3.11 the variation of β_h for low and high qualities is plotted for low and moderate pressures. Fig. 3.12 shows the calculated data on β_h for high pressures. It is found that a constant value of β_h is reasonable for moderate changes in quality. In contrast, the variation in the thermal expansion coefficient for single-phase water is shown in Fig. 3.13. Comparing the nature of variation given in Figs. 3.11 and 3.12 with Fig. 3.13, it appears that for a two-phase steam−water mixture, the error introduced by considering constant thermal expansion coefficient for small ranges of quality is similar to that for single-phase water for small ranges of temperature.

Problem 2: Having seen that the plot of density given by Eq. (3.31) is identical to Eq. (3.37), show that the density relation expressed by Eq. (3.31) is identical to the density expression Eq. (3.37) for homogeneous two-phase flow.

3.3.4 Open-loop two-phase natural circulation systems

By definition, an open-loop NCS is one that exchanges both energy and mass with the surroundings. With this definition, there are two types of open loops possible, as shown in Fig. 3.14. As you can see, Fig. 3.14A is a physically closed loop, whereas Fig. 3.14B is a physically open loop. In the case

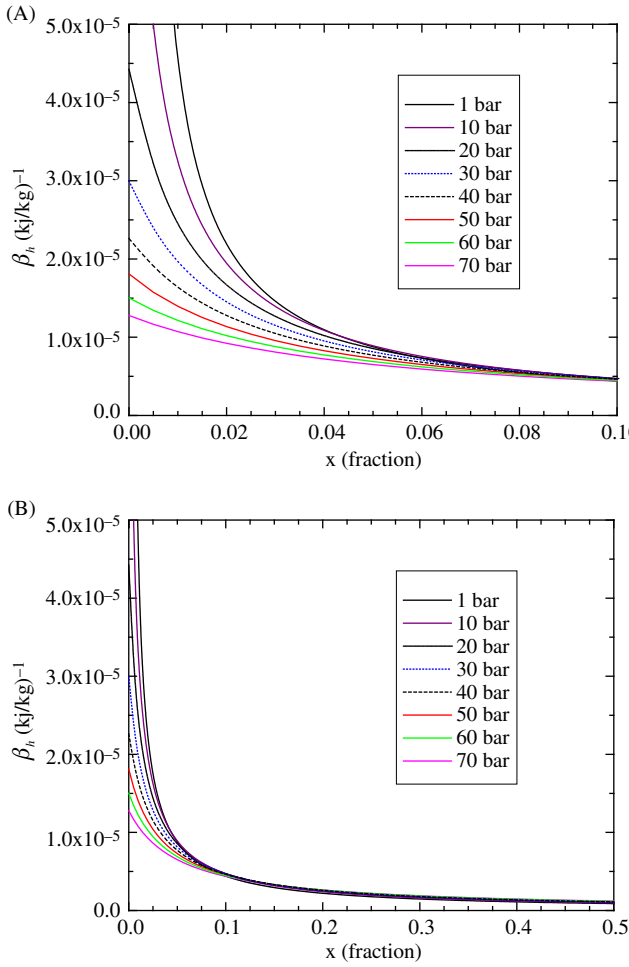

FIGURE 3.11 β_h variation for water at moderate pressures for low and high qualities: (A) β_h variation at low qualities; (B) β_h variation at high qualities.

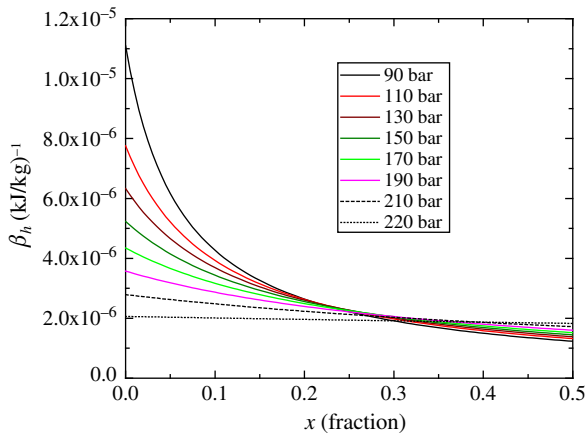

FIGURE 3.12 β_h variation for water at high pressures.

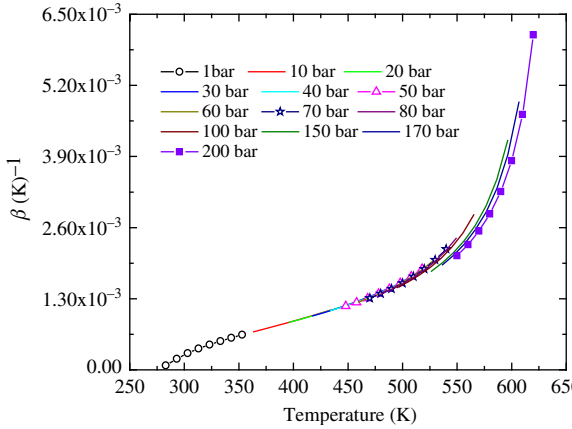

FIGURE 3.13 β_T variation for single-phase water.

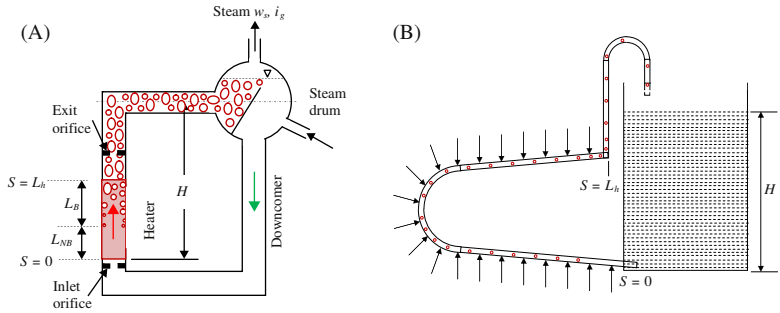

FIGURE 3.14 Different open-loop two-phase natural circulation systems: (A) physically closed loop: (B) physically open loop.

of Fig. 3.14A, the mass and momentum conservation equations remain the same as Eqs. (3.34) and (3.35). For the loop shown in Fig. 3.14B, although the mass equation remains the same as Eq. (3.34), the integral momentum equation can be written as

$$\frac{L_t}{A}\frac{\partial w}{\partial t} + \frac{1}{A^2}\int_{s=0}^{L_t} \partial\left(w^2 v\right) + P_o - P_i + \frac{fL_t w^2}{2D\rho A^2} + g\rho_o\beta_h \int_{s=0}^{L_t} i\partial z = 0 \qquad (3.41)$$

Since there is no heat sink for both loops shown in Fig. 3.14, the energy equation can be written as

$$\frac{\partial(\rho i)}{\partial t} + \frac{1}{A}\frac{\partial(wi)}{\partial s} = \left\{ \begin{array}{ll} \dfrac{4q_h}{D} & \text{heater for } 0 < s \le L_h \\ 0 & \text{for pipes } L_h < s \le L_{hl} \text{ and } L_{hl} < s \le L_t \end{array} \right\} \qquad (3.42)$$

If the feed water flow rate and its inlet temperature are specified, then an energy balance at the steam drum would give the inlet enthalpy of the downcomer.

$$w(1-x)i_f + w_F i_F - w i_{in} = V_{SD}\frac{\partial(\rho i)}{\partial t} \tag{3.43}$$

where V_{SD} is the steam drum volume. Also, for open loops, the mass flow rate of steam is assumed to be equivalent to that of the feed flow rate. However, in the case of Fig. 3.14A, the loop circulation rate can be several times the feed flow rate. For both figures, the thermodynamic equilibrium is assumed to calculate the nonboiling length L_{NB} and the boiling length L_B.

3.3.5 Supercritical closed-loop natural circulation systems

One of the issues of supercritical fluids is the sharp change in properties near the critical point (see Fig. 3.15). This sharp change in properties continues much beyond the pseudocritical point (i.e., the point at which the specific heat is maximum).

The thermal expansion coefficient variation calculated from the density using the relationship in Eq. (3.16b) is plotted in Fig. 3.16. It may be emphasized here that the sharp variation of properties, especially in the near-critical and pseudocritical regions, makes it difficult to apply the Boussinesq approximation, which helped to simplify the analysis of subcritical single-phase natural circulation loops.

The Boussinesq approximation, however, may be valid in the deeply supercritical region as is evident from the property variations shown in Figs. 3.15 and 3.16. Ambrosini and Sharabi (2008) have shown that a unique relationship applicable for all supercritical fluids exists between the dimensionless density ρ^* and the dimensionless enthalpy i^*. Ambrosini and Sharabi (2008) defined ρ^* and i^* as below:

$$\rho^* = \rho/\rho_{pc} \text{ and } i^* = \beta_{pc}\left(i - i_{pc}\right) \tag{3.44}$$

Swapnalee et al. (2012) tested this with various fluids such as water, CO_2, Freon-12, and Freon-114, as shown in Fig. 3.17. The interesting fact about this relationship is that this is almost independent of pressure and fluid in the supercritical region. Swapnalee et al. (2012) found that this is indeed true for their test data, as shown in Fig. 3.18 for supercritical water and CO_2. Using the dimensionless density in Eq. (3.7), the momentum equation can be written as

$$\rho_{pc}\frac{\partial(\rho^* u)}{\partial t} + \rho_{pc}\frac{\partial(\rho^* uu)}{\partial s} + \frac{\partial P}{\partial s} + \frac{f\rho_{pc}\rho^* u^2}{2D} + \rho_{pc}\rho^* g\sin\theta = 0 \tag{3.45}$$

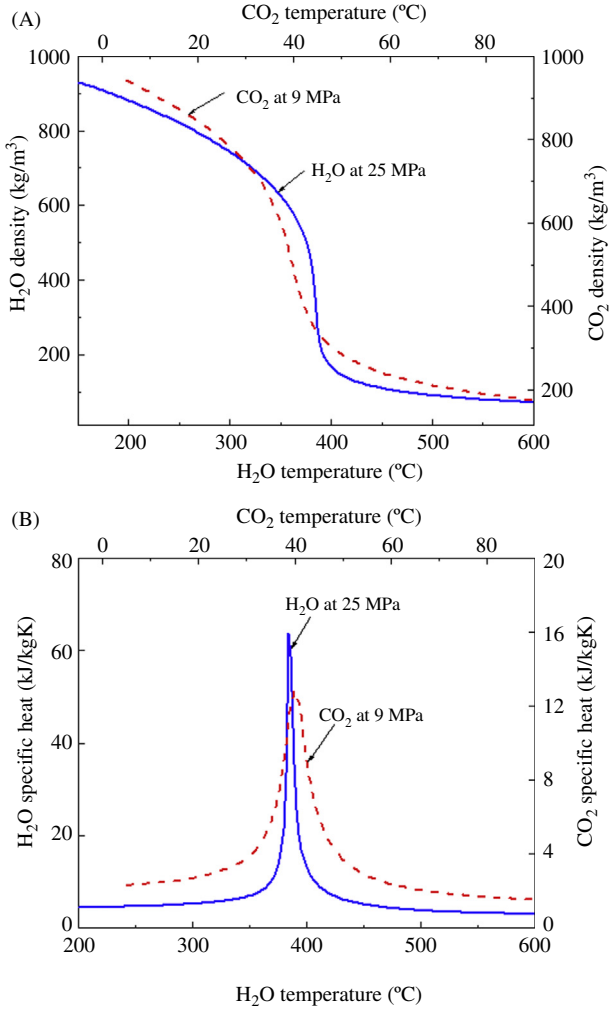

FIGURE 3.15 Variation of density and specific heat of supercritical water and CO_2 in the near-critical and pseudocritical region: (A) density variation; (B) specific heat variation.

Swapnalee et al. (2012) have shown that linear relationships can be fitted to the three regions with steep property variation (see also Fig. 3.18) of the form

$$\rho^* = C_1 - C_2 i^* \tag{3.46}$$

Using the definition of ρ^* and i^*, the conservation of mass (i.e., Eq. 3.3) can be rewritten as

$$\frac{\partial \rho^*}{\partial t} + \frac{\partial (\rho^* u)}{\partial s} = 0 \tag{3.47}$$

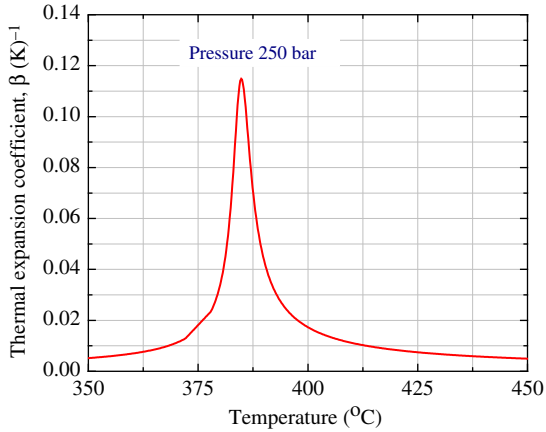

FIGURE 3.16 Variation of thermal expansion coefficient for supercritical water in the near-critical and supercritical region.

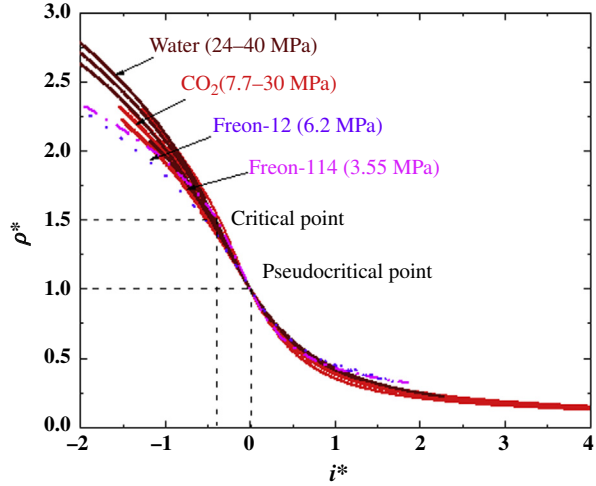

FIGURE 3.17 Comparison of dimensionless density as functions of dimensionless enthalpy for CO_2, water, Freon-12, and Freon-114.

Similarly, using the linear relationship between ρ^* and i^* (i.e., Eq. 3.46), the integral momentum equation for a closed loop can be written as

$$L_t \rho_{pc} \frac{\partial(\rho^* u)}{\partial t} + \frac{f L_t \rho_{pc} \rho^* u^2}{2D} + \rho_{pc} g C_2 \oint i^* dz = 0 \tag{3.48}$$

Linear relationships of the type shown in Eq. (3.46) for the three regions shown in Fig. 3.15 differ in the value of the constants C_1 and C_2, leading to

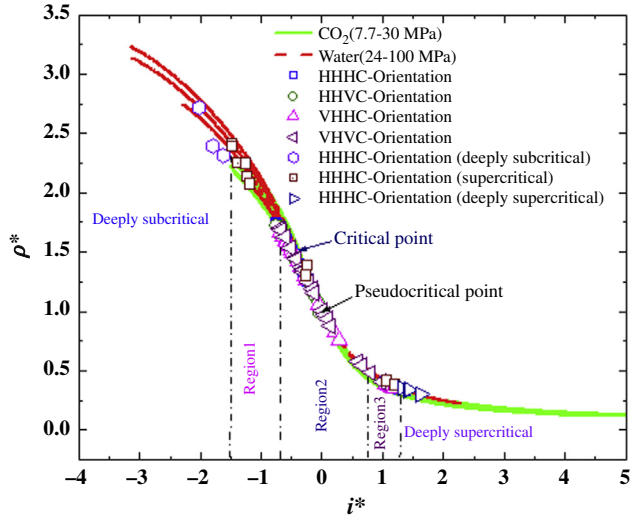

FIGURE 3.18 Experimental data on dimensionless density and dimensionless enthalpy plot (CO_2 and water data).

different equations for the different regions. The energy conservation Eq. (3.30) can be modified in terms of i^* as

$$\frac{\rho_{pc}}{\beta_{pc}}\frac{\partial(\rho^* i^*)}{\partial t}+\frac{\rho_{pc}}{\beta_{pc}}\frac{\partial(\rho^* u i^*)}{\partial s} = \begin{cases} \dfrac{4q_h}{D} & \text{for heater } 0<s\le s_h \\ 0 & \text{for pipes } s_h<s\le s_{hl} \text{ and } s_c<s\le s_t \\ -\dfrac{4U_i(T-T_s)}{D} & \text{for cooler } L_{hl}<s\le L_c \end{cases} \tag{3.49}$$

These equations can be rewritten in terms of the mass flow rate w ($w = \rho A u$) as

$$\rho_{pc}\frac{\partial\rho^*}{\partial t}+\frac{1}{A}\frac{\partial w}{\partial s}=0 \tag{3.50}$$

$$\frac{L_t}{A}\frac{\partial w}{\partial t}+\frac{fL_t(w)^2}{2D\rho_{pc}\rho^* A^2}+\rho_{pc}gC_2\oint i^* dz=0 \tag{3.51}$$

$$\frac{\rho_{pc}}{\beta_{pc}}\frac{\partial(\rho^* i^*)}{\partial t}+\frac{1}{A\beta_{pc}}\frac{\partial(w i^*)}{\partial s} = \begin{cases} \dfrac{4q_h}{D} & \text{for heater } 0<s\le s_h \\ 0 & \text{for pipes } s_h<s\le s_{hl} \text{ and } s_c<s\le s_t \\ -\dfrac{4U_i(T-Ts)}{D} & \text{for cooler } s_{hl}<s\le s_t \end{cases} \tag{3.52}$$

3.3.6 Supercritical open-loop natural circulation system

In the case of open loop NCS, the mass equation remains the same and the momentum equation can be integrated to obtain

$$\frac{L_t}{A}\frac{\partial w}{\partial t} + \frac{1}{A^2\rho_{pc}}\int_{s=0}^{L_t}\partial\left(w^2 v^*\right) + \frac{fL_t}{2DA^2\rho_{pc}\rho^*}\frac{w^2}{} + P_o - P_i - g\rho_{pc}\int_{s=0}^{L_t}\rho^* dz = 0 \tag{3.53}$$

Replacing ρ^* using Eq. (3.46) the momentum equation can be integrated. The energy equation gets modified as

$$\frac{\rho_{pc}}{\beta_{pc}}\frac{\partial\left(\rho^* i^*\right)}{\partial t} + \frac{1}{A\beta_{pc}}\frac{\partial\left(wi^*\right)}{\partial s} = \left\{\begin{array}{ll}\dfrac{4q_h}{D} & \text{for heater } 0 < s \le s_h \\ 0 & \text{for pipes } s_h < s \le s_t\end{array}\right\} \tag{3.54}$$

3.4 Constitutive relations

The governing equations described above involve terms like friction factor, loss coefficient and heat transfer coefficient. In addition, these also involve fluid properties which are to be obtained from the equation of state for the working fluid in the system. These are known as constitutive relations and knowledge of these relations is required for solving the governing equations described above. In addition, certain natural circulation phenomena like instability can be influenced by phenomena like flow pattern transitions. Instability can also induce premature critical heat flux (CHF), especially during the low-flow period of the oscillation cycle. Hence background knowledge of these phenomena is essential for better understanding and analysis of the NCS.

Depending on whether the loop considered is single-phase, two-phase, or supercritical, the constitutive equations for friction and heat transfer are different. Also, since the field is very vast, in many instances only the reference for the constitutive equations is given for brevity.

3.4.1 Friction factor

The friction factor is basically used to estimate the pressure loss due to wall friction in fluid dynamic systems. Since the equations used for the friction pressure loss are different for single-phase and two-phase flows, separate discussion is provided for the two cases.

3.4.1.1 Single-phase isothermal systems

The friction coefficient depends on a large number of parameters such as the flow regime (laminar, transition, or turbulent), nature of the flow (developing or fully developed), flow geometry (circular, annular, rectangular, rod bundle, etc.), surface roughness, diabatic or adiabatic flow and the dimensionless

Reynolds number. In general, friction factor correlations for fully developed isothermal flow conditions in a circular pipe are reasonably well-established and are used for the analysis of natural circulation loops. Employing the hydraulic diameter concept, the same correlations are used for noncircular geometries. Well-established procedures exist to account for the surface roughness effect on the friction factor. These are briefly described here with suggestions for their application to natural circulation loops.

Laminar flow regime

For circular pipes, the equation for the Darcy−Weisbach friction coefficient for fully developed laminar flow is given by

$$f = \frac{64}{Re} \tag{3.55}$$

Transition flow regime

In this regime, although a few friction factor correlations are reported (Knudson and Katz, 1958), universally acceptable equations are not available. For the analysis of natural circulation loops, we recommend the use of the correlation given by Swapnalee and Vijayan (2011), which was based on the transition region data from natural circulation tests. The correlation is reproduced below.

$$f = \frac{1.2063}{Re^{0.416}} \tag{3.56}$$

This correlation is compared with various turbulent flow correlations extrapolated to the transition regime in Fig. 3.19. As seen from the figure, its prediction is reasonable and the difference could be due to the developing nature of the flow in the experimental natural circulation loop.

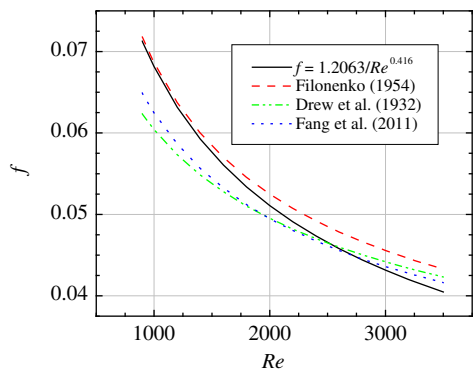

FIGURE 3.19 Comparison of friction factor predicted by Eq. (3.56) with various correlations.

Turbulent flow regime

For the fully developed turbulent flow regime, several friction factor correlations are reported in the literature. A few important ones among them are given below:

$$f = \frac{0.316}{Re^{0.25}} \text{ Blasius correlation valid for } 3000 < Re \le 2 \times 10^4 \tag{3.57}$$

For $2 \times 10^4 < Re \le 2 \times 10^6$, the Blasius correlation (see Fang et al., 2011) is given by

$$f = \frac{0.184}{Re^{0.2}} \tag{3.58}$$

The following correlation proposed by Nikuradse (1933) is valid for the entire range of Reynolds number for turbulent flow in smooth pipes

$$\frac{1}{\sqrt{f}} = 2\log\left(Re\sqrt{f}\right) - 0.8 \tag{3.59}$$

For fully developed turbulent flow in rough pipes, Von Karman (1930) proposed the following equation

$$\frac{1}{\sqrt{f}} = 2\log\,(D/e) + 1.74 \tag{3.60}$$

The above equation is valid in the range $(D/e)/(Re\sqrt{f_f}) > 0.01$, where e is the absolute roughness and f_f is the Fanning friction factor (equals one-fourth of Darcy–Weisbach friction factor used in this text). Colebrook (1938) combined Eqs. (3.59) and (3.60) and proposed the following correlation applicable for turbulent flow in smooth and rough pipes valid over the Reynolds number range of $4000 < Re \le 10^8$.

$$\frac{1}{\sqrt{f}} = -2\log\left(\frac{e/D}{3.71} + \frac{2.52}{Re\sqrt{f}}\right) \tag{3.61}$$

This equation is the basis of the Moody's chart commonly used for estimation of the friction factor and is valid in the transition and fully developed turbulent flow regimes for both smooth and rough tubes. Note that friction factor appears on the LHS as well as RHS of Eqs. (3.59) and (3.61). Therefore, an iterative procedure is required while calculating the friction factor by these equations which is not desirable for use in computer codes as it increases the computational time. To overcome this issue, explicit forms of the Colebrook and Nikuradse friction factor correlations are proposed by various authors (Selander, 1978; Chen, 1979; Goudar and Sonnad, 2003; and several others). A review and assessment of the explicit friction factor correlations can be found in Chen (1979), Yildirim (2009), Brkic (2011), Genic et al. (2011), and Fang et al. (2011). Based on the assessment by Fang et al.

(2011), the Filonenko (1954) correlation is a good approximation of the Colebrook equation for smooth tubes in the range of $10^4 < Re \leq 10^8$. The correlation is given by

$$f = [0.79 \ln Re - 1.64]^{-2} \tag{3.62}$$

Fang et al. (2011) provided the following explicit equation for the Colebrook correlation applicable for smooth and rough tubes valid in the range $3000 < Re \leq 10^8$ and $0 < \varepsilon \leq 0.05$.

$$f = 1.613\left[\ln\left(0.234\varepsilon^{1.1007} - \frac{60.525}{Re^{1.1105}} + \frac{56.291}{Re^{1.0712}}\right)\right]^{-2} \tag{3.63}$$

where ε is the relative roughness defined as e/D. For numerical prediction of transients such as start up from rest as well as instability with repeated flow reversals, often it is required to use friction factor correlations valid for laminar, transition, and turbulent regimes. When flow regime switching occurs it is essential to have continuity of predicted friction factor values for avoiding numerical instability and to obtain a converged solution. If only laminar and turbulent flows are considered, then the switching can be continuous if one uses the following condition

$$f = Max\,(f_l, f_t) \tag{3.64}$$

This means that the friction factor is to be calculated by both the laminar and the turbulent flow correlations and the higher value is chosen for further calculation. However, this leads to the laminar to turbulent flow transition at $\sim Re = 1200$, which is acceptable in the interest of obtaining a numerical solution. Also, there are experimental indications from simple loop facilities that the laminar to turbulent flow transition takes place at lower Reynolds numbers for natural circulation flow (Creveling et al., 1975; Bau and Torrance, 1981).

Often, it may be required to consider all three flow regimes for natural circulation flow transients like start-up from rest and instability with repetitive flow reversals. The latter may involve variation of Reynolds number from −10,000 to 10,000, even in simple rectangular loops (Vijayan et al., 1995). In such cases the transition correlation Eq. (3.56) given by Swapnalee and Vijayan (2011) can be used along with the equations for laminar and turbulent flows. As shown in Fig. 3.20, no discontinuity is observed in the friction factor predictions if we use the condition

$$f = Max(f_l, f_{tr}, f_t) \tag{3.65}$$

As can be seen from Fig. 3.20, the friction factor continuity demands switching from laminar to transition flow at $Re = 898$ and from transition to turbulent flow at $Re = 3196$.

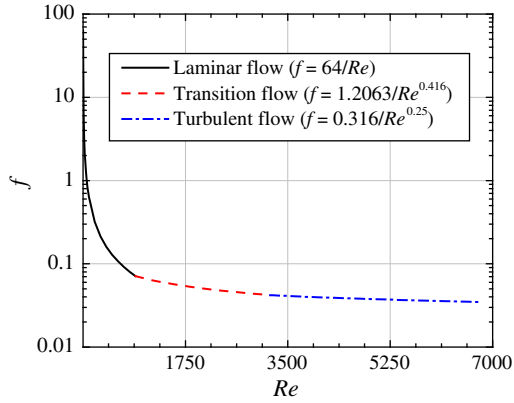

FIGURE 3.20 Friction factor predictions by the laminar, transition, and turbulent flow correlations.

Nonisothermal single-phase flow

The nonisothermal nature of the flow is accounted for by multiplying the isothermal friction factor with a correction coefficient, F. The following empirical equation is given for the correction factor, F

$$F = \left(\frac{\mu_b}{\mu_w}\right)^{-n} \tag{3.66}$$

where the subscripts b and w refer to the bulk fluid and wall, respectively. The value of n reported is different by different authors and it varies from 0.14 (Kays and Crawford, 1993) to 0.28 (Leung and Groeneveld, 1991). The generally accepted value is 0.14.

The early experiments indicated the friction coefficient in natural circulation to be different from that for forced convection (Bau and Torrance, 1981; Creveling et al., 1975). Natural circulation experiments under laminar flow by Hallinan and Viskanta (1986) showed that forced convection friction factor relations are adequate to model fluid friction. Currently, the friction factor correlations developed for fully developed forced convective flow are considered applicable to natural circulation flow. It may introduce some error, especially due to three-dimensional effects and the best way to eliminate this is to generate the forced convection friction factor data for the expected range of Reynolds number in natural circulation flow. Generally, such data are generated as part of the test loop characterization (see Fig. 3.21) with the same pipe dimensions used in the test facility.

The higher measured value in the above figure is due to the surface roughness of the commercial pipe used in the experiments.

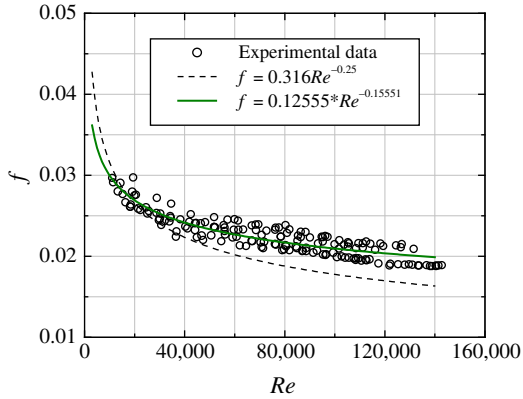

FIGURE 3.21 Typical measured friction factor data compared with Blasius correlation.

Noncircular geometries

Noncircular geometries of simple shape as well as complex shapes like rod bundles are also of interest for nuclear power plants.

Simple noncircular shapes

Analytical friction factor equations for fully developed laminar flow in many noncircular conduits are available. For example, Kays and Crawford (1993) present fully developed laminar flow friction factor equations for simple noncircular geometries such as rectangular, square, triangular and annular flow ducts. For fully developed turbulent flow in noncircular geometries, the hydraulic diameter concept is used in the calculation of Reynolds number to estimate the friction factor from equations applicable to circular pipe.

Rod bundles

The fuel rod bundles used in BWRs, PWRs, PHWRs and FBRs are vastly different. Both BWRs and PWRs use long vertical fuel bundles (length varying from 1.8 to 4.5 m) with grid-type spacers, whereas PHWRs use short bundles ($\sim$0.5 m long) with split-wart-type spacers stacked one after another in a horizontal fuel channel. The FBRs also use long bundles with wire-wrap-type spacers. The hydraulic diameter concept is not considered valid for certain geometries like the nuclear fuel rod bundle and the friction factor is estimated as

$$f = f_{cp} K_1 \tag{3.67}$$

where f_{cp} is the friction factor calculated using circular pipe correlations and the correction factor K_1 is provided as a function of the p/D (pitch to diameter) ratio (Diessler and Taylor, 1956). For most rod bundles, experimental

determination of single-phase friction factor for the particular geometry may be inevitable. Such a study for CANDU-type PHWR bundles has been carried out by Snoek and Ahmad (1983) and Vijayan et al. (1999). While friction factor correlations for the turbulent flow can be found in Snoek and Ahmad (1983), the study by Vijayan et al. (1999) gives friction factors covering the laminar, transition, and turbulent ranges. A generalized method for estimation of friction factor for wire-wrapped fuel bundles is given by Rehme (1968, 1969).

3.4.1.2 *Two-phase systems*

There are several models for the estimation of friction pressure loss in two-phase systems. These are broadly categorized into homogeneous flow models, models based on the two-phase friction multiplier, and flow pattern-specific models. In addition, there are direct empirical models which are not very popular and are not described here.

Homogeneous flow models

Here the friction factor is calculated using the same equations applicable for single-phase flow with the use of a two-phase viscosity in the estimation of the Reynolds number. There are a large number of homogeneous models reported in the literature which differ only in the models used for the estimation of two-phase viscosity. Some of the reported models for two-phase viscosity are given in Table 3.1.

Homogeneous flow models are expected to give good results for high mass flux two-phase flows [$> 2700\,\text{kg/m}^2$ as per Hussain et al. (1974)] where the bubble diameter is small compared to the duct diameter.

TABLE 3.1 Two-phase viscosity models.

S. no.	Author	Two-phase viscosity model
1	McAdams et al. (1942)	$\frac{1}{\mu_{tp}} = \frac{x}{\mu_g} + \frac{1-x}{\mu_f}$
2	Cicchitti et al. (1960)	$\mu_{tp} = x\mu_g + (1-x)\mu_f$
3	Owens (1961)	$\mu_{tp} = \mu_f$
4	Dukler et al. (1964)	$\mu_{tp} = \alpha\mu_g + (1-\alpha)\mu_f$, where α is given by Eq. (3.39)
5	Beattie and Whalley (1982)	$\mu_{tp} = \alpha\mu_g + \mu_f(1-\alpha)\,(1+2.5\alpha)$, where α is given by Eq. (3.39)

Two-phase friction multiplier model

Here the two-phase friction factor is obtained by multiplying the single-phase friction factor by a two-phase friction multiplier. Several definitions of two-phase friction multipliers exist and the most commonly used definition is given below.

$$\phi_{LO}^2 = \frac{(dp/ds)_{TPF}}{(dp/ds)_{LO}} \tag{3.68}$$

where the LHS is the friction multiplier, the numerator is the two-phase flow pressure drop per unit length and the denominator corresponds to pressure drop per unit length in the same duct under single-phase saturated liquid conditions with mass flow rate equal to the total mixture mass flow rate.

A large number of two-phase multiplier models exist. The commonly used models are those due to Martinelli-Nelson (1948), Lockhart-Martinelli (1949), Lottes-Flinn (1956), Thom (1964), Baroczy (1966), Becker et al. (1962), and Chisholm (1973). The reader may refer to IAEA-TECDOC-1203 (2001) for a full description of the two-phase friction multiplier models.

Flow pattern-specific model

Two-phase flow can have a large number of flow patterns which depend on the orientation of the flow geometry. For example, vertical two-phase flow can be bubbly, slug, churn, annular, or droplet flow. Similarly, horizontal two-phase flow can be bubbly, stratified, slug, annular, or droplet flow. The orientation brings about some subtle changes even though with regard to structure the same flow pattern exists in horizontal and vertical flow. For example, stratified flow known as vertical stratification occurs in relatively large-diameter vertical riser pipes of two-phase NCSs at low mass fluxes. In addition, the annular flow in horizontal tubes can have more thickness at the bottom compared to that at the top wall. The friction pressure drop in two-phase flow depends on the type of flow pattern encountered. Also, these flow pattern-specific correlations are not well-established as the multiplier-based models. However, certain natural circulation phenomena such as flow pattern transition instability require flow pattern-specific pressure drop correlations (Nayak et al., 2003). Commonly used flow pattern-specific correlations for vertical and horizontal flow are given in IAEA-TECDOC-1203.

One of the issues associated with multiplier-based and flow pattern-specific models is that the continuity of pressure drop in the single-phase liquid (i.e., at $x = 0$) and single-phase vapor (i.e., at $x = 1$) may not be maintained. The continuity of pressure drop as flow pattern switches from one to another is not necessarily met by the flow pattern-specific pressure drop correlations. Therefore, one must be careful while using them in system computer codes.

Diabatic two-phase flow

The discussions thus far have dealt with adiabatic two-phase flow. In the case of diabatic two-phase flow, the quality and the void fraction vary along the length of a heated or cooled pressure drop test section. There are conflicting opinions on the effect of heat flux on the two-phase friction pressure drop. For example, Koehler and Kastner (1988) concluded that the two-phase pressure drop is the same in heated and unheated channels, whereas Tarasova et al. (1966) observed that two-phase pressure drop in heated channels is greater than that in unheated channels. Leung et al. (1993) indicated that the effective surface roughness increases in heated channels, leading to a larger pressure drop. However, a well-established procedure to account for this effect is not yet available.

There are two general approaches to calculate pressure drop in diabatic test sections. In the first approach, an integrated value of the two-phase friction multiplier over the entire heated test section is calculated as

$$\phi_{LO}^2 = \frac{1}{L_t}\int_0^{L_t} \phi_{LO}^2(z)dz \tag{3.69}$$

This approach is applicable if the friction multiplier for diabatic two-phase flow is an integrable function. In fact, such integrated friction multipliers are presented as a function of exit quality and pressure for steam−water flow by Thom (1964) and Martinelli-Nelson (1948). The second approach subdivides the diabatic test section into a number of smaller segments and using the mean value of quality, void fraction, and flow pattern in each segment, the friction multiplier is calculated using the adiabatic two-phase friction models described above.

In diabatic two-phase test sections, often the inlet condition corresponds to single-phase liquid flow and hence a model is required to calculate the single-phase length. Frequently, analysts use the thermodynamic equilibrium model for this case. However, thermodynamic nonequilibrium exists in heated channels and hence many analysts (Marinelli and Pastori, 1973; Vijayan et al., 1981; Snoek and Ahmad, 1983) use the Saha and Zuber (1974) model to account for this. For rod bundles, Snoek and Leung (1989) found that the original Saha and Zuber correlation is inadequate and modified it to predict the onset of nucleate boiling.

The measured pressure drop in diabatic two-phase flow in both vertical and horizontal test sections includes the acceleration pressure drop. In the case of vertical flows, the measured pressure drop also includes the elevation pressure drop. As both these depend on the two-phase density which in turn depends on the void fraction, the choice of the void fraction correlation becomes important for the calculation of two-phase pressure drop.

Recommendations on two-phase pressure drop correlations

From the above, it is clear that many different types of two-phase pressure drop correlations exist and often the designers and analysts need some guidance on which correlation to use. The best option here is to examine the various reported assessments of these correlations and their recommendations. Several assessments of two-phase friction factor models have been conducted in the past which can be classified into two types. The first assesses two-phase pressure drop data disregarding the flow pattern to which the data belong as the vast majority of reported two-phase flow pressure drop data do not mention the flow pattern to which the data belong. The second is based on flow pattern-specific pressure drop data which require a preassessment of the flow pattern transition criteria or flow pattern maps. Important among the first category are the assessments by Idsinga et al. (1977), Friedel (1979, 1980), Beattie and Whalley (1982), Snoek and Leung (1989), and Lombardi and Carsana (1992). The assessments of the second type are due to Mandhane et al. (1977), Hashizume and Ogawa (1987), and Behnia (1991).

Homogeneous model

Beattie and Whalley (1982) used the HTFS (Heat Transfer and Fluid Flow Services) databank consisting of 13,500 adiabatic data points (8400 horizontal and 5100 vertical pipe) to assess 12 correlations including five homogeneous pressure drop models. Since the measured pressure drop also included the elevation pressure drop in the case of vertical two-phase flow data, the homogeneous void fraction model was used to calculate the elevation pressure drop in the case of homogeneous models and an unpublished void fraction correlation was used to calculate the elevation pressure drop for the other pressure drop models. They conclude that the homogeneous models are as good as the others in predicting two-phase pressure drop.

Eighteen two-phase pressure drop models including four homogeneous models were included in the assessment of 3500 steam–water adiabatic and diabatic two-phase pressure drop data mostly for vertical two-phase flow by Idsinga et al. (1977). The HEM was used to calculate the single-phase length in the case of diabatic data. Also, the homogeneous void fraction model was used to calculate the elevation pressure drop in the case of homogeneous pressure drop models and in the case of other pressure drop models, the void fraction consistent with the original proposal was used. They obtained best predictions from the homogeneous models proposed by Owens (1961) and Cicchitti et al. (1960). These correlations included in the assessment of Beattie and Whalley (1982) gave good predictions, although not as good as those of Beattie and Whalley (1982) correlation.

Multiplier-based model

The assessment using a databank of 9000 points by Dukler et al. (1964) included five correlations (Baker, 1954; Bankoff, 1960; Chenoweth and Martin, 1956; Lockhart-Martinelli, 1949; Yagi 1954) and Lockhart-Martinelli was the best of these five. Idsinga et al. (1977) assessed 14 multiplier-based models and the recommended models were those due to Baroczy (1966) and Thom (1964). Friedel (1980) assessed 14 multiplier-based models using 12,868 adiabatic two-phase flow data points and found Chisholm (1973) and Lombardi-Pedrochi (1972) DIF-1 correlations to be the best-performing ones.

Flow pattern-specific models

The flow pattern maps used in the various reported assessments are different. For example, Mandhane et al. (1977) and Behnia (1991) used Mandhane et al. flow pattern map, whereas Weisman and Choe (1976) used their own flow pattern map. Weisman and Choe (1976) used the AGA-API databank for their assessment of flow pattern-specific correlations for horizontal two-phase flow which considered the four flow patterns of separated flow (stratified flow), intermittent flow (slug flow), annular flow, and homogeneous flow. Based on their assessment, they recommend Agrawal et al. (1973) and Hoogendoorn (1959) correlations for separated flow, Dukler et al. (1964), Lockhart-Martinelli (1949), and Hughmark (1965) correlations for slug flow, Dukler et al. (1964) and Lockhart-Martinelli (1949) correlations for annular flow and McAdams et al. (1942), Dukler et al. (1964), and Chisholm (1968) correlations for homogeneous flow. Mandhane et al. used the University of Calgary pipe flow databank to assess 16 pressure drop correlations. Their assessment considered six flow patterns for horizontal two-phase flow. They recommended Chenoweth and Martin (1956) correlation for bubbly and elongated bubbly flow, Agrawal et al. (1973) for stratified flow, Dukler et al. (1964) for stratified wavy, Mandhane et al. (1974) for slug flow, Chenoweth and Martin (1956) for annular and annular mist flow, and Mandhane et al. (1974) for dispersed flow. Hashizume and Ogawa (1987) carried out an assessment using a modified Baker (1954) map with selected data points (2281) from HTFS databank including some very low mass flux data to assess five correlations and concluded that their correlation gave the best predictions for refrigerant data.

For diabatic two-phase flow in CANDU-type horizontal rod bundles an assessment of nine correlations was carried out by Snoek and Leung (1989) using 1217 data points with the modified Saha-Zuber (1974) correlation to identify the onset of nucleate boiling which also considered acceleration pressure drop due to density change. The Friedel (1979) correlation predicted the data best, while the Beattie and Whalley (1982) model was found to result in small errors.

Assessment of natural circulation pressure drop and void fraction data

Note that the two-phase natural circulation involves diabatic (i.e., heated or cooled) test sections. Vijayan et al. (2000) compiled steam−water pressure drop and void fraction data for two-phase natural circulation loops from the open literature and made an assessment of both the friction and void fraction correlations. The assessment considered 14 friction pressure drop and 33 void fraction correlations. The void fraction correlations were initially screened out using the three limiting conditions (i.e., at $x = 0$, $\alpha = 0$, at $x = 1$, $\alpha = 1$, and at critical pressure $\alpha = x$). Only 8 of the 33 correlations were found to satisfy all the 3 limiting conditions and 14 of the 33 correlations were found to satisfy at least 2 limiting conditions (i.e., at $x = 0$, $\alpha = 0$ and at $x = 1$, $\alpha = 1$). These 14 correlations were then assessed using 2611 void fraction data and found that Chexal et al. (1996) correlation gave the best prediction, closely followed by Osmachkin-Borisov (1970), Rouhani (1969), Thom (1964), and Bankoff-Jones (1960) correlations. Subsequently, using the Chexal et al. (1996) void fraction correlation and the Saha and Zuber correlation for onset of subcooled boiling, the 14 pressure drop correlations were assessed which included three homogeneous models. Both the homogeneous and the multiplier-based models were selected based on recommendations of previous assessments. This assessment showed that all the pressure drop correlation predictions were close to each other, with the best prediction from Lockhart-Martinelli (1949) correlation, followed by Lottes-Flinn (1956) and Sekoguchi et al. (1970). Interestingly, both the homogeneous model and multiplier-based models performed well.

3.4.1.3 Supercritical systems

In general, single-phase friction factor correlations are used for the supercritical NCSs. For example, Pioro and Duffey (2007) use the Filonenko (1954) correlation for the estimation of friction factor for supercritical fluids.

3.4.2 Local loss coefficients

Local pressure losses are important to NCSs. These are the irreversible pressure losses that occur at locations of flow area change, flow direction change, flow obstructions, etc. The local pressure losses are calculated as

$$\Delta P = K \frac{\rho u^2}{2} \tag{3.70}$$

where K is the local loss coefficient. Generally, the local loss coefficients depend on the flow regime and the type of local cross-section change (sudden expansion, contraction, orifice, etc.), direction change (45 and 90 degrees elbows, U-bend, V-bend, S-bend, Tee, etc., are examples), etc.

Local losses also occur at many of the components of rod bundles such as the inlet and outlet tie plates and spacers. In a CANDU-type fuel channel, the alignment of two adjacent bundles can differ, causing a local pressure loss at the junction between bundles. Minimization of system pressure losses (both friction as well as local losses) is important to enhance the flow rate and hence the heat transport capability in NCSs. Knowledge of the local pressure losses is therefore important to designers and analysts of NCSs.

3.4.2.1 Single-phase systems

The loss coefficients of commonly encountered flow obstructions such as orifices, sudden contraction and sudden expansion, elbows, U-bends, etc., can be found in Idelchik (1986). However, the loss coefficient data for many special components which exist in rod bundles of nuclear power plants need to be generated experimentally. For many nonstandard pipe components also, the loss coefficient data may be required to be generated experimentally. In such cases, the loss coefficient data are given as a function of the Reynolds number (see Fig. 3.22). For fully developed turbulent flow, the loss coefficient becomes a constant beyond a certain Reynolds number, as shown in Fig. 3.22, and often only this constant value is reported in literature. Hence, frequently it becomes necessary to generate local loss coefficient data, as shown in Fig. 3.22, for the natural circulation loop under study.

Loss coefficient correlations of general validity are difficult to find for the various components of pressure drop in rod bundles. A generalized method, however, for grid spacers is proposed by Rehme (1973,1977). Loss coefficient correlations specific to the bundles used can be found from

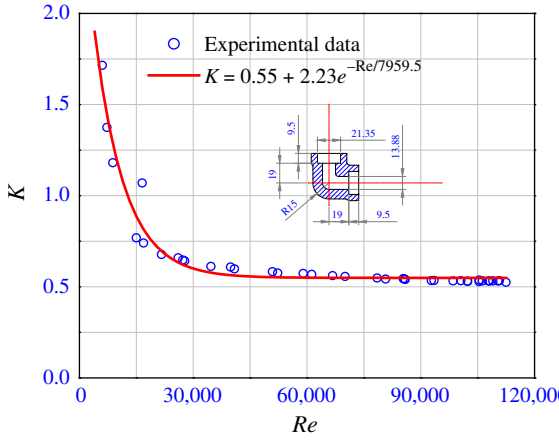

FIGURE 3.22 Variation of loss coefficient in a short radius elbow.

various authors (Mochizuki and Shiba, 1986; Kim et al., 1992). Loss coefficient correlations specific to components of CANDU-type fuel bundles, including that for the bundle alignment at the junction between two fuel bundles, can be found in Vijayan et al. (1999).

3.4.2.2 Two-phase systems

In general, the homogeneous or the slip model is used to predict the local pressure loss in two-phase flow. As per the homogeneous model, the two-phase local pressure loss is estimated as

$$\Delta P = K(Re_{sat})\frac{\rho u^2}{2} \tag{3.71}$$

where $K(Re_{sat})$ is estimated using single-phase correlations corresponding to the Reynolds number calculated assuming the total flow rate to be liquid at saturated conditions. The density for the two-phase mixture is calculated using the homogeneous model (Eqs. 3.37 and 3.39). As per the slip model, the local pressure loss coefficient for two-phase flow can be expressed as

$$K_{TPF} = K_{SPF}\frac{\rho_f}{\rho} \tag{3.72}$$

where the two-phase density (the denominator in the above equation) is calculated using Eq. (3.37) with the void fraction calculated using Eq. (3.38). Grillo and Marinelli (1970) recommend a value of 2 for the slip ratio for calculating the two-phase flow loss coefficient for grid spacers.

3.4.2.3 Supercritical systems

Due to lack of data, the loss coefficients for supercritical fluids are assumed to be same as for single-phase fluids.

3.4.3 Heat transfer coefficients

For natural circulation loops, it is often required to calculate the heat transfer coefficients at the heat source and the heat sink. The heat transfer coefficient correlations for the source and sink are different for single-phase, two-phase and supercritical fluids.

3.4.3.1 Single-phase flow

The heat transfer coefficient under single-phase flow conditions depends on the geometry, flow regime and boundary conditions. In the case of isothermal wall boundary conditions, the fully developed constant property laminar flow heat transfer coefficient for a circular pipe is given by

$$Nu = 3.656 \tag{3.73}$$

For uniform heat flux, the fully developed constant property laminar flow heat transfer coefficient for a circular pipe is given by

$$Nu = 4.364 \tag{3.74}$$

Note that for developing flow at the tube entrance, the Nusselt number value will be somewhat higher than those given by Eqs. (3.73) and (3.74). For simple noncircular geometries, such as rectangles, with different aspect ratios, ellipses, triangles, hexagons, etc., the heat transfer coefficient under fully developed laminar flow is given in various books (Kays and Crawford, 1993; Thirumaleshwar, 2006). Most of the analytical solutions given in the literature are for constant property flow. In the case of variable properties, the following relationship given in Kays and Crawford (1993) is found to be useful to predict the Nusselt number.

$$\frac{Nu}{Nu_{cp}} = \left(\frac{\mu_w}{\mu_m}\right)^n \tag{3.75}$$

Note that Nu_{cp} is the Nusselt number at constant properties and μ_w and μ_m are the viscosities corresponding to the wall and mix mean temperature. The value of the exponent "n" given by different investigators is different. However, a value of -0.14 is commonly used.

For transition flow, well-established correlations are not available. For fully developed turbulent flow in circular pipes, the widely used Dittus–Boelter correlation to calculate the heat transfer coefficient is given by

$$Nu = 0.023\, Re^{0.8}\, \mathrm{Pr}^{0.4} \tag{3.76}$$

where the physical properties of the fluid are calculated at the bulk temperature. For a large temperature change across the film, the physical property most affected is the viscosity and the Sieder-Tate (1936) equation is often used to account for this and is given by

$$Nu = 0.023\, Re^{0.8}\, \mathrm{Pr}^{0.4} \left(\frac{\mu_w}{\mu_b}\right)^{0.14} \tag{3.77}$$

Here again the fluid properties are evaluated at the bulk temperature, excepting μ_w which is estimated corresponding to the wall temperature. For noncircular conduits, circular tube correlations are used with the hydraulic diameter concept to estimate the heat transfer coefficient. Again, continuity of heat transfer coefficients as flow regime changes from laminar to transition and transition to turbulent regimes are required for numerical computations.

For accounting for the heat losses from the insulated pipes of natural circulation loops, often estimation of natural convection heat transfer coefficients is also required. In many instances of NCSs, the heat sink is basically a heat exchanger immersed in a large pool in which case also estimation of single-phase natural convective heat transfer coefficient is required. In

addition, many of the advanced reactor systems use liquid metals such as sodium, lead and lead bismuth eutectic as coolants. Correlations for the heat transfer coefficient for natural convection and liquid-metal coolants are well-established and are beyond the scope of this book.

3.4.3.2 Two-phase flow heat transfer

Both boiling and condensation heat transfer are important for two-phase natural circulation loops. Generally, boiling heat transfer occurs at the source in the case of two-phase NCLs and on the secondary side of the heat sink in single-phase NCSs relevant to PWRs. During certain transients with reduced primary side inventory, condensation heat transfer can occur in the primary side of steam generators (i.e., the heat sink).

Boiling heat transfer

With subcooled single-phase liquid entering a heated tube, several heat transfer regimes exist as shown in Fig. 3.23 starting with the single-phase forced convective heat transfer regime (Collier, 1981). For this regime, the heat transfer coefficients for single-phase fully developed flow can be used as given in Section 3.4.3.1. The correlations applicable for subcooled boiling, saturated boiling, and forced convective boiling are described below.

Subcooled boiling: In the subcooled boiling region, the bulk temperature of the liquid is less than saturation. The Saha and Zuber model is use to estimate the length of the subcooled boiling regime. Chen's (1963) correlation applicable for subcooled boiling region is given by

$$h_{sub} = h_{mac} + h_{mic} \tag{3.78}$$

where $h_{mac} = h_{DB}$, and $h_{mic} = h_{FZ}S$. Note that h_{FZ} and h_{DB} are, respectively, the heat transfer coefficients evaluated by the Forster−Zuber and Dittus−Boelter correlations, and S can be calculated using single-phase Reynolds number with $x = 0$ as

$$S = \left(1 + 2.53 \times 10^{-6} Re_f^{1.17}\right)^{-1} \tag{3.79}$$

The Jens and Lottes (1951) correlation is also widely used for calculating the heat transfer coefficient in the subcooled boiling region and is given by

$$h_{sub} = \left[\frac{e^{P/62}}{25}\right] (\Delta T_{sat})^3 \tag{3.80}$$

Saturated boiling

For the saturated boiling region, a number of correlations (more than 30) are available. Important among them are Chen (1966), Kandlikar (1990), Shah (1982), Bjorge et al. (1982), and Gungor and Winterton (1987). Only the first two correlations are described here.

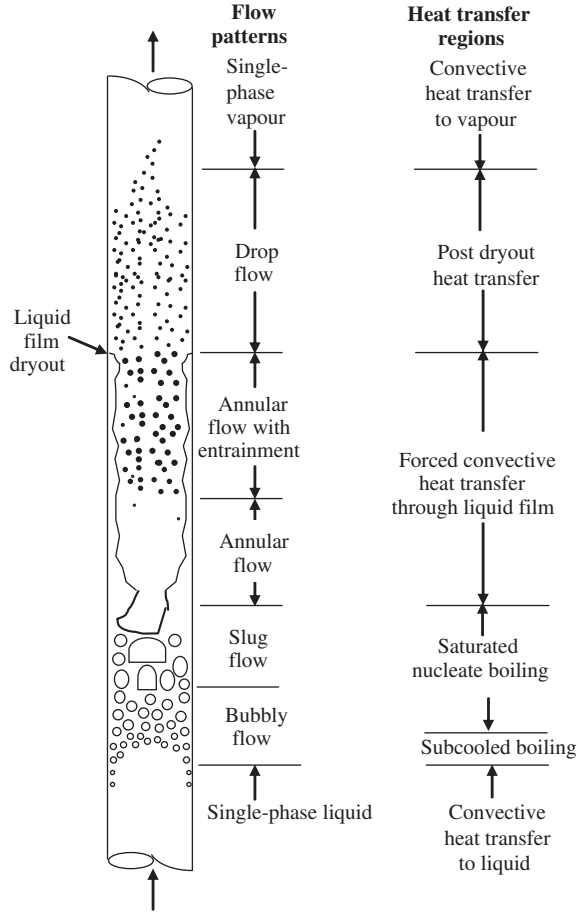

FIGURE 3.23 Flow patterns and heat transfer regimes in vertical two-phase flow.

Kandlikar correlation (1990)

This correlation is applicable to the nucleate boiling and the forced convective regions. The correlation is given by

$$\frac{h_{tp}}{h_f} = C_1 Co^{C_2} (25 Fr_{LO})^{C_5} + C_3 Bo^{C_4} F_{FL} \tag{3.81}$$

where

$$Co = \left(\frac{1-x}{x}\right)^{0.8} \left(\frac{\rho_g}{\rho_f}\right)^{0.5} \quad ; \quad Bo = \frac{q_h}{G i_{fg}} \quad \text{and} \quad Fr_{LO} = \frac{G^2}{\rho_f^2 g D} \tag{3.82}$$

Co is the convection number, Bo the boiling number and h_f = single-phase heat transfer coefficient with only the liquid fraction flowing in the tube. The Dittus−Boelter equation is used to calculate h_f. The values of constants C_1−C_5 are given in Table 3.2. Table 3.3 gives the values of the fluid-dependent parameters F_{FL}.

TABLE 3.2 Constants in the proposed correlation (Eq. 3.81).

Constant	Convective region	Nucleate boiling region
C_1	1.1360	0.6683
C_2	− 0.9	− 0.2
C_3	667.2	1058.0
C_4	0.7	0.7
C_5[a]	0.3	0.3

[a] *$C_5 = 0$ for vertical tubes, and for horizontal tubes with $Fr_{LO} > 0.04$.*

TABLE 3.3 Fluid-dependent parameter F_{FL} in the proposed correlation (Eq. 3.81).

Fluid	F_{FL}
Water	1.00
R-11	1.30
R-12	1.50
R-1381	1.31
R-22	2.20
R-113	1.30
R-114	1.24
R-152a	1.10
Nitrogen	4.70
Neon	3.50

The two sets of values given in Table 3.2 correspond to the convective boiling and nucleate boiling regions, respectively. The heat transfer coefficient at any given condition is evaluated using the two sets of constants for the two regions, and since the transition from one region to another occurs at the intersection of the respective correlations, the higher of the two heat transfer coefficient values represents the predicted value.

Chen correlation (1966)

This correlation also includes both heat transfer coefficients due to nucleate boiling as well as forced convective mechanisms.

$$h_{tp} = h_{mic} + h_{mac} \tag{3.83}$$

where h_{mic} is the nucleate boiling part and h_{mac} is the convective part

$$h_{mic} = h_{FZ}\, S \tag{3.84}$$

$$h_{mac} = h_{DB}\, F \tag{3.85}$$

S and F are functions of Re_L and χ_{tt} (the Martinelli parameter), respectively. The suppression factor S is the ratio of the effective superheat to wall superheat and can be calculated using Eq. (3.79). It accounts for decreased boiling heat transfer because the effective superheat across the boundary layer is less than the superheat based on wall temperature. The enhancement factor F is a function of the Martinelli parameter χ_{tt} and is given by

$$F = 1 \quad \text{for} \frac{1}{\chi_{tt}} \leq 0.1 \tag{3.86}$$

$$F = 2.35\left(\frac{1}{\chi_{tt}} + 0.213\right)^{0.736} \quad \text{for} \quad \frac{1}{\chi_{tt}} > 0.1 \tag{3.87}$$

The Forster–Zuber correlation (1955) is given by

$$h_{FZ} = 0.0012\left(\frac{k_f^{0.79} Cp_f^{0.045} \rho_f^{0.49} g^{0.25}}{\sigma^{0.5} \mu_f^{0.29} i_{fg}^{0.24} \rho_g^{0.24}}\right) \Delta T_w^{0.24} \Delta P^{0.75} \tag{3.88}$$

where $\Delta T_w = T_w - T_{sat}$ and $\Delta P = P_{\text{wall temperature}} - P$

Dry out

The annular liquid film dry out is also referred to as CHF. A large number of empirical correlations exist for annular film dry out. This in itself denotes the inadequacy of CHF correlations. Most thermal hydraulic codes currently use the look up table (LUT) approach to predict the CHF (Groeneveld et al., 1996). CHF-LUT is a three-dimensional table expressing normalized CHF data for an 8-mm inside diameter tube as a function of pressure, quality, and mass flux. The LUT has a wide application range (0.1–20 MPa, 0–8000 kg/m^2/s, and −50 to 100% in quality), which is better than any correlation. It has a correction factor to account for the diameter effect for application to tubes of diameter other than 8 mm. In addition, it uses correction factors for noncircular geometries like rod bundles, spacers, etc. A complete description of these can be found in IAEA-TECDOC-1203.

Post dry out heat transfer

The heat transfer region after the liquid film dry out is often referred to as the post dry out (PDO) or post CHF heat transfer region. It includes both transition boiling and film boiling. In transition boiling there is intermittent

wetting, while in film boiling the heater surface is too hot to permit liquid contact. Due to the poor heat transfer through the vapor, very high heater surface temperature is encountered in film boiling which could lead to burnout of the heater. Surface temperature oscillations are expected in transition boiling. Prediction of the post CHF heater surface temperature requires heat transfer correlations which are empirical in nature.

In the high-quality region most of the heat transferred during transition boiling is due to the droplet-wall interaction. Just after CHF the surface temperature is low enough to facilitate droplet deposition, whereas at high wall superheats droplets could be repelled before contacting the heater surface. Although NCSs are designed to prevent CHF and post CHF heat transfer region during normal operation, it may be encountered during a LOCA. Furthermore, one should differentiate between pool film boiling and flow film boiling. Many heat transfer regions exist, such as inverted annular film boiling (IAFB), dispersed flow film boiling (DFFB), and even radiation heat transfer becomes important as the surface temperature can be very high.

In this region also, there is a proliferation of correlations and the uncertainty in the prediction of post CHF heat transfer is more than that in the prediction of CHF. Even in this case there is an attempt to generate a look up table the same way for CHF LUT although it has not matured to the same level. A full description of the methodology to estimate the PDO heat transfer can also be found in IAEA-TECDOC-1203. As per this document, the recommended correlation for pool film boiling for horizontal surfaces is the modified Bromley equation given below

$$Nu_{FB} = 0.62\left[\frac{k_g^3\rho_g\left(\rho_f-\rho_g\right)i_{fg}g}{\Delta T_s\mu_g}\frac{1}{2\pi}\sqrt{\frac{g\left(\rho_f-\rho_g\right)}{\sigma}}\right]^{\frac{1}{4}} \tag{3.89}$$

The film boiling look up table is recommended for flow film boiling region.

Single-phase heat transfer to vapor

Dittus–Boelter-type correlation is used in this region. Similar correlations are recommended for heat transfer to superheated vapor [an example is given in Miropolskiy (1975)].

Condensation heat transfer

Condensation heat transfer can be important in two-phase natural circulation loops if the heat sink is a condenser. This is true for most two-phase NCSs used for computer cooling. In addition, the loops relevant to PWRs, VVERs, and PHWRs also can operate in the boiler-condenser mode for certain transients as indicated earlier. In addition, condensation heat transfer is important

for a natural circulation-based passive containment cooling system (PCCS) and the isolation condenser system in advanced reactors. For PCCS, condensation in the presence of noncondensables is also important.

3.4.3.3 Supercritical heat transfer

Since phase change and CHF are eliminated in supercritical fluids, the fuel design in SCWR is governed by a clad temperature limit. Hence accurate prediction of the heat transfer coefficient assumes significance in SCWR design. However, the heat transfer phenomenon in supercritical fluids is complicated due to the possibility of the occurrence of heat transfer deterioration around the critical point. Far away from the pseudocritical point, the heat transfer coefficient approaches that given by the Dittus–Boelter correlation which is known as the normal heat transfer region in supercritical fluids. In addition, an enhanced heat transfer region also occurs in the pseudoboiling region, which occurs below the pseudocritical point. The heat transfer deterioration occurs due to the occurrence of pseudofilm boiling above the pseudocritical temperature.

Heat transfer in supercritical fluids can be affected by a number of parameters such as flow regime (laminar, turbulent), geometry (tubes, annuli, rod bundles, etc.), magnitude of heat flux and its profile, and the magnitude of the flow and its direction (vertical upward, downward, or horizontal flow). Even supercritical natural circulation loops usually operate in the turbulent flow regime and hence laminar flow heat transfer correlations applicable to supercritical fluids are not reported in the literature. Most of the heat transfer correlations reported till now are based on experimental investigations, although correlations based on CFD studies are emerging. A compilation of the supercritical heat transfer database can be found in IAEA-TECDOC-1746 (2014). Most of the reported correlations are for tubes and have the general form given by the Dittus–Boelter correlation with various modifications suggested. Again, a large number of correlations exist. Wang et al. (2010) assessed four supercritical correlations using the AECL tube database and the best prediction was obtained with the modified Krasnoschekov–Protopov correlation described in Jackson (2002). The Yang and Khartabil (2005) and the Jackson (2002) correlations gave comparable predictions. An assessment by Kuang et al. (2008) considered a large number of supercritical correlations using the SJTU database. All assessed correlations predicted a peak in heat transfer coefficient in the vicinity of the pseudocritical point (although there were differences in the peak value) and far away from the pseudocritical point all predictions were similar. The following correlation proposed by Mokry et al. (2011) is suggested by Pioro et al. (2016).

$$Nu_b = 0.0061 \mathrm{Re}_b^{0.904}\ \mathrm{Pr}\ 0.684 \left(\frac{\rho_w}{\rho_b}\right)^{0.564} \tag{3.90}$$

It must be mentioned here that universally acceptable correlation for the supercritical region is still not available.

3.4.4 Equation of state

Equation of state is also required to make meaningful computations for NCSs. In the case of single-phase loops, we require density, viscosity, thermal conductivity, specific heat, and thermal expansion coefficient as a function of temperature. Two-phase and supercritical loops need additional data. Most computer codes used today have steam–water properties built in, generally based on the IAPWS R7-97 (2012) formulation. Many of the advanced and the generation IV nuclear reactors under development need properties of fluids like supercritical water, helium, liquid metals like sodium, lead, and lead bismuth eutectic, and a variety of molten salts. In addition, simulant fluids are often used in certain instances, especially in test facilities for ease of experimentation. Further, the supercritical CO_2-based Brayton cycle is proposed for power conversion in generation IV reactors instead of the Rankine cycle presently used. Properties of helium, supercritical CO_2, and supercritical water are available from the NIST fluid property database (NIST, 2010). The properties of liquid-metal coolants used in generation IV reactors are available from Sobolev (2010). Other sources of liquid sodium and LBE properties are the Handbook of Thermodynamic and Transport Properties of Alkali Metals (1985), Fink and Leibowitz (1995), and the LBE Handbook (2015). Natural circulation-based high-temperature solar thermal power plants use molten salt containing a eutectic mixture of sodium and potassium nitrates. Thus, properties of a large number of molten salts are required for analysis of NCSs relevant to nuclear reactors and solar thermal power plants. Molten salt properties are available from Janz (1967), Khokhlov et al. (2009), and Serrano-Lopez et al. (2013).

3.5 Closure

The governing equations applicable for one-dimensional single-phase, two-phase, and supercritical NCSs have been derived from the first principles with commonly used assumptions. Governing equations for both closed-loop and open-loop NCSs have been described. In addition, the constitutive relations for friction and heat transfer are presented for single-phase, two-phase, and supercritical natural circulation loops along with recommendations based on previous assessments. The sources for the equation of state for commonly used fluids in nuclear reactor systems have also been described.

Nomenclature

A	flow area, m^2
b	exponent in Eq. (3.18)
Bo	boiling number (q_h/Gi_{fg})
Cp	specific heat, J/(kg K)
Co	convection number, $\left[(1-x)/x\right]^{0.8}\left(\rho_g/\rho_f\right)^{0.5}$
D	diameter, m
e	absolute roughness, m
f	friction factor
Fr_{LO}	Froude number with total flow as liquid $\left(G^2/\left(\rho_f^2 gD\right)\right)$
g	acceleration due to gravity, m/s^2
G	mass flux, $kg/(m^2s)$
h	heat transfer coefficient, W/m^2K
i	enthalpy, J/kg
i^*	dimensionless enthalpy, $\left(\beta_{pc}(i-i_0)\right)$
k	thermal conductivity, W/(mK)
K	loss coefficient
L	length, m
Nu	Nusselt number, $\left(hD/k\right)$
p	constant in Eq. (3.18)
P	pressure, Pa
Pr	Prandtl number $\left(Cp\mu/k\right)$
q	heat flux, W/m^2
q_c	heat flux due to conduction, W/m^2
Re	Reynolds number $\left(Dw/A\mu\right)$
s	coordinate along the loop, m
S	slip ratio u_g/u_f
t	time, s
T	temperature, K
ΔT_{sat}	difference between wall temperature and saturation temperature
u	velocity, m/s
U	overall heat transfer coefficient, $W/(m^2K)$
v	specific volume, m^3/kg
V	volume, m^3
w	mass flow rate, kg/s
x	quality
z	elevation, m

Subscripts

0	reference
a	ambient
b	bulk
c	cooler
cp	circular pipe

DB Dittus−Boelter
f saturated liquid
fg vapor minus liquid
FZ Forster−Zuber
g saturated vapor or gas
h heater
hl hot leg
LO liquid only
mac macro
mic micro
pc pseudocritical
s secondary
sat saturation
SD steam drum
sp single-phase
sub subcooled
t total
tt turbulent-turbulent
tp two-phase
w wall

Greek symbols

α void fraction
α_d thermal diffusivity, m^2/s
β_T thermal expansion coefficient, 1/K
β_h thermal expansion coefficient, kg/J
Δ refers to difference
ε relative roughness (e/D)
θ angle between the flow direction and the horizontal
χ Martinelli parameter
μ dynamic viscosity, kg/(ms)
ξ perimeter, m
ρ density, kg/m^3
ρ^* dimensionless density, $\left(\rho/\rho_{pc}\right)$
σ surface tension, N/m
τ shear stress, N/m^2
ϕ_{LO}^2 two-phase friction multiplier

List of acronyms used

AC alternating current
AECL Atomic Energy of Canada Limited
API American Petroleum Institute
BWR boiling water reactor
CANDU Canadian deuterium uranium reactor
CFD computational fluid dynamics
CHF critical heat flux

DFM drift flux model
DFFB dispersed flow film boiling
FBR fast breeder reactor
HEM homogeneous equilibrium model
HHHC horizontal heater horizontal cooler
HHVC horizontal heater vertical cooler
HTFS heat transfer and fluid flow services
HX heat exchanger
IAEA International Atomic Energy Agency
IAFB inverted annular film boiling
IAPWS International Association for Properties of Water and Steam
LBE lead bismuth eutectic
LHS left-hand side
LOCA loss of coolant accident
LUT look up table
NC natural circulation
NCL natural circulation loop
NCS natural circulation system
NIST national institute of standards and technology
PCCS passive containment cooling system
PDO post dry out
PHWR pressurized heavy-water reactor
PWR pressurized-water reactor
SBO station blackout
SCWR supercritical water reactor
SJTU Shanghai Jiao Tong University
TFM two-fluid model
VHHC vertical heater horizontal cooler
VHVC vertical heater vertical cooler
VVER Russian PWR with vertical core and horizontal steam generator

References

Agrawal, S.S., Gregory, G.A., Govier, G.W., 1973. An analysis of stratified two-phase flow in pipes. Can. J. Chem. Eng. 51, 280–286.

Ambrosini, W., Sharabi, M., 2008. Dimensionless parameters in stability analysis of heated channels with fluids at supercritical pressures. Nucl. Eng. Design 238, 1917–1929.

Baker, O., 1954. Simultaneous flow of oil and gas. Oil Gas J. 53, 185.

Bankoff, S.G., 1960. A variable density single-fluid model for two-phase flow with particular reference to steam-water flow. J. Heat Transfer 82, 265–272.

Baroczy, C.J., 1966. A systematic correlation for two-phase pressure drop. Chem. Eng. Progr. Symp. Ser 62, 232–249.

Bau, H.H., Torrance, K.E., 1981. Transient and steady state behavior of an open symmetrically heated free convection loop. Int. J. Heat Mass Transfer 24, 597–609.

Beattie, D.R.H., Whalley, P.B., 1982. A simple two-phase frictional pressure drop calculation method. Int. J. Multiphase Flow 8, 83–87.

Becker, K.M., Hernborg, G., Bode, M., 1962. An experimental study of pressure gradients for flow of boiling water in vertical round ducts. (part 4) AE-86.

Behnia, M., 1991. Most accurate two-phase pressure drop correlation identified. Oil Gas J. 90–95.

Bjorge, R.W., Hall, G.R., Rohsenow, W.M., 1982. Correlation of forced convection boiling heat transfer data. Int. J. Heat Mass Transfer 25, 753–757.

Brkic, D., 2011. Review of explicit approximations to the Colebrook relation for flow friction. J. Petrol. Sci. Eng. 77, 34–48.

Chen, J.C., 1963. A Correlation for Boiling Heat Transfer to Saturated Fluid in Convective Flow. ASME Paper 63-HT-34.

Chen, J.C., 1966. A correlation for boiling heat transfer to saturated fluids in convective flow. Ind. Eng. Chem. Process Design Dev. 5 (3), 322–329.

Chen, N.H., 1979. An explicit equation for friction factor in pipe. Ind. Eng. Chem. Fundam. 18, 296–297.

Chenoweth, J.M., Martin, M.W., 1956. Pressure drop of gas-liquid mixtures in horizontal pipes. Petrol. Eng. 28, C-42-45.

Chexal, B., Maulbetsch, J., Santucci, J., Harrison, J., Jensen, P., Peterson, C., Lellouche, G., Horowitz, J., 1996. Understanding void fraction in steady and dynamic environments. TR-10636/RP-8034-14, Electric Power Research Institute, 3412 Hillview Avenue, Palo Alto, California.

Chisholm, D., 1968. The influence of mass velocity on friction pressure gradient during steam-water flow. In: Proc. Thermodynamics and Fluid Mechanics Conf., Institute of Mechanical Engineers, 182, 336–341.

Chisholm, D., 1973. Pressure gradients due to friction during the flow of evaporating two-phase mixtures in smooth tubes and channels. Int. J. Heat Mass Transfer 16, 347–358.

Cicchitti, A., Lombardi, C., Silvestri, M., Soldaini, G., Zavattarelli, R., 1960. Two-phase cooling experiments: pressure drop, heat transfer and burnout experiments. Energia Nucleare 7, 407–425.

Colebrook, C.F., 1938. Turbulent flow in pipes with particular reference to the transition region between the smooth and rough pipe laws. J. Inst. Civil Eng 11, 133–156. 1938/1939.

Collier, J.G., 1981. Convective Boiling and Condensation. McGraw-Hill, London.

Creveling, H.F., De Paz, J.F., Baladi, J.Y., Schoenhals, R.J., 1975. Stability characteristics of a single-phase free convection loop. J. Fluid Mech. 67, 65–84.

Dukler, A.E., Wicks, M., Cleveland, R.G., 1964. Frictional pressure drop and holdup in two-phase flow, Part A – a comparison of existing correlations for pressure drop and holdup, B – An approach through similarity analysis. AIChE J. 10, 38–43. and 44–51.

Diessler, G., Taylor, M.F., 1956, Analysis of axial turbulent flow heat transfer through banks of rods or tube, Reactor Heat Transfer Conference, TID-7529, vol. 2.

Fang, X., Xu, Y., Zhou, Z., 2011. New correlations of single-phase friction factor for turbulent pipe flow and evaluation of existing single-phase friction factor correlations. Nucl. Eng. Design 241, 897–902.

Filonenko, G.K., 1954. Hydraulic resistance in pipes. Teploenergetika. 1, 40 (Russian).

Fink, J.K., Leibowitz, L., 1995. Thermodynamic and transport properties of sodium liquid and vapor, ANL/RE-95/2, Reactor Engineering Division, Argonne National Laboratory, USA.

Forster, H.K., Zuber, N., 1955. Dynamics of vapour bubbles and boiling Heat Transfer. J. AIChE 1, 531–535.

Friedel, L., 1979. Improved friction pressure drop correlations for horizontal and vertical two-phase flow. European two-phase flow group meeting, Ispra.

Friedel, L., 1980. Pressure drop during gas/vapor-liquid flow in pipes. Int. Chem. Eng. 20, 352–367.

Gartia, M.R., Vijayan, P.K., Pilkhwal, D.S., 2006. A generalized flow correlation for two-phase natural circulation loops. Nucl. Eng. Design 236, 1800–1809.

Genic, S., Arandjelovic, I., Kolandic, P., Jaric, M., Budimir, N., Genic, V., 2011. A review of explicit approximations of Colebrook's equation. FME Trans. 39, 67–71.

Goudar, C.T., Sonnad, J.R., 2003. Explicit friction factor correlation for turbulent flow in smooth pipes. Ind. Eng. Chem. Res. 42, 2878–2880.

Grillo, P., Marinelli, V., 1970. Single and two-phase pressure drops on a 16-ROD bundle. Nucl. Applicat. Technol. 9, 682–693.

Groeneveld, D.C., et al., 1996. The 1996 look-up table for critical heat flux in tubes. Nucl. Eng. Design *1631–23*.

Gungor, K.E., Winterton, R.H.S., 1987. Simplified general correlation for saturated flow boiling and comparisons of correlations with data. Canad. J. Chem. Eng. 65, 148–156.

Hallinan, K.P., Viskanta, R., 1986. Heat transfer from a rod bundle under natural circulation conditions. U.S. Nuclear Regulatory Commission, NUREG/CR-4556, TI86 901126, Washington, DC.

Handbook of thermodynamic and transport properties of alkali metals, 1985. Chemical data series no.30 (Int. Union of Pure and Applied Chemistry – IUPAC), Blackwell Scientific publications.

Hashizume, K., Ogawa, N., 1987. Flow pattern, void fraction and pressure drop of refrigerant two-phase flow in horizontal pipe — III Comparison of the analysis with existing pressure drop data on air/water and steam/water systems. Int. J. Multiphase Flow 13, 261–267.

Hoogendoorn, C.J., 1959. Gas-liquid flow in horizontal pipes. Chem. Eng. Sci. 9, 205–217.

Hughmark, G.A., 1965. Holdup and heat transfer in horizontal slug gas-liquid flow. Chem. Eng. Sci. 20, 1007–1010.

Hussain, A., Choe, W.G., Weisman, J., 1974. The Applicability of the Homogeneous Flow Model to Pressure Drop in Straight Pipe and Across Area Changes. COO-2152-16.

IAEA-TECDOC-1203, 1203. Thermalhydraulic Relationships for Advanced Water-Cooled Reactors. IAEA, Vienna, pp. 274–280, ISSN 1011-4289.

IAEA-TECDOC-1746, 2014. Heat Transfer Behavior and Thermalhydraulics Code Testing for Supercritical Water Cooled Reactors (SCWRs). IAEA-TECDOC Series, ISSN 1011-4289.

IAPWS R7-97 (2012), 2007. Revised Release on the IAPWS Industrial Formulation 1997 for the Thermodynamic Properties of Water and Steam.

Idelchik, I.E., 1986. Hand Book of Hydraulic Resistances. Hemisphere Publishing Company, New York.

Idsinga, W., Todreas, N., Bowring, R., 1977. An assessment of two-phase pressure drop correlations for steam-water mixtures. Int. J. Multiphase Flow 3, 401–413.

Jackson, J.D., 2002. Consideration of the heat transfer properties of supercritical pressure water in connection with the cooling of advanced nuclear reactors. In: Proceedings of 13th Pacific Basin Nuclear Conference, October 21–25, Shenzhen City, China.

Janz, G.J., 1967. Molten Salts Handbook. Academic Press Inc, New York.

Jens, W.H., Lottes, P.A., 1951. Analysis of Heat Transfer, Burnout, Pressure Drop and Density Data for High Pressure Water. ANL-4627.

Kandlikar, S.G., 1990. A general correlation for saturated two-phase flow boiling heat transfer inside horizontal and vertical tubes. J. Heat Transfer Vol. 112, 219–227.

Kays, W.M., Crawford, M.E., 1993. Convective Heat and Mass Transfer, third ed. McGraw-Hill Inc, Singapore, pp. 79–82.

Khokhlov, V., Ignatiev, V., Afonichkin, V., 2009. Evaluating physical properties of molten salt reactor fluoride mixtures. J. Fluorine Chem. 130, 30–37.

Kim, N.-H., Lee, S.K., Moon, K.S., 1992. Elementary model to predict the pressure loss across a spacer grid without a mixing vane. Nucl. Technol. 98, 349–353.

Knudson, J.G., Katz, D.L., 1958. Fluid dynamics and heat transfer. International Student Edition. McGraw-Hill Book Company, New York, pp. 146–212.

Koehler, W., Kastner, W., 1988. In: Kakac, S., Bergles, A.E., Fernandes, E.O. (Eds.), Two-Phase Pressure Drop in Boiler Tubes, Two-Phase Flow Heat Exchangers: Thermalhydraulic Fundamentals and Design. Kluwer Academic Publishers.

Kuang, B., Zhang, Y.Q., Cheng, X., 2008. A new wide-ranged heat transfer correlation of water at supercritical pressures in vertical upward ducts. In: Proc. 7th International Topical Meeting on Nuclear Reactor Thermal Hydraulics, Operation and Safety (NUTHOS-7), Seoul, Korea, October 5–9, paper 189.

LBE Handbook, NEA No. 7268, ©OECD 2015.

Leung, L.K.H., Groeneveld, D.C., 1991. Frictional pressure gradient in the pre- and post-CHF heat transfer regions. Multiphase flows'91, Tsukuba, Japan.

Leung, L.K.H., Groeneveld, D.C., Aube, F., Tapucu, A., 1993. New studies of the effect of surface heating on frictional pressure drop in single-phase and two-phase flow. NURETH-3, Grenoble, France.

Lockhart, R.W., Martinelli, R.C., 1949. Proposed correlation of data for isothermal two-phase, two-component flow in pipes. Chem. Eng. Prog. 45, 39–48.

Lombardi, C., Pedrochi, E., 1972. A pressure drop correlation in two-phase flow. Energia Nucleare 19 (2), 91–99.

Lombardi, C., Carsana, C.G., 1992. A dimensionless pressure drop correlation for two-phase mixtures flowing upflow in vertical ducts covering wide parameter ranges. Heat Technol. 10, 125–141.

Lottes, P.A., Flinn, W.S., 1956. A method of analysis of natural circulation boiling systems. Nucl. Sci. Eng. 192, 91–99.

Mandhane, J.M., Gregory, G.A., Aziz, K., 1974. A flow pattern map for gas-liquid flow in horizontal pipes. Int. J. Multiphase Flow 1, 537.

Mandhane, J.M., Gregory, G.A., Aziz, K., 1977. Critical evaluation of friction pressure-drop prediction methods for gas-liquid flow in horizontal pipes. J. Petrol. Technol. 29, 1348–1358.

Marinelli, V., Pastori, L., 1973. AMLETO – a pressure drop computer code for LWR fuel bundles. RT/ING(73)11, Comitato Nacionale Energia Nucleare (CNEN).

Martinelli, R.C., Nelson, D.B., 1948. Prediction of pressure drop during forced circulation boiling of water. Trans. ASME 70, 695–702.

McAdams, W.H., Woods, W.K., Heroman Jr., R.H., 1942. Vaporisation inside horizontal tubes. II. Benzene-oil mixtures. Trans. ASME 64, 193.

Miropolskiy, Z.L., 1975. Heat transfer to superheated steam at heat supply and heat removal. Teploenergetika 3, 75–78. in Russian.

Mochizuki, H., Shiba, K., 1986. Characteristics of natural circulation in the ATR plant. In: 2nd Int. Top. Mtg. Nuclear Power Plant Thermal Hydraulics and Operations, Tokyo, pp. 132–139.

Mokry, S., Gospodinov, Y.E., Pioro, I., Kirillov, P., 2011 Supercritical water heat-transfer correlation for vertical bare tubes, Proceedings of the 17th International Conference on Nuclear Engineering ICONE-17, Brussels, Belgium, July 12-16, Paper # 76010 (2009) 8 pages.

National Institute of Standards and Technology, 2010. NIST Reference Fluid Thermodynamic and Transport Properties – REFPROP. NIST Standard Reference Database 23, Ver. 9.1, Department of Commerce, Boulder, CO.

Nayak, A.K., Vijayan, P.K., Jain, V., Saha, D., Sinha, R.K., 2003. Study on the flow-pattern-transition instability in a natural circulation heavy water moderated boiling light water cooled reactor. Nucl. Eng. Design 225, 159–172.

Nikuradse, J., 1933. Stroemungsgesetze in rauhen Rohren. Ver. Dtsch. Ing. Forsch 361, 1–22.

Osmachkin, V.S., Borisov, V., 1970. Pressure drop and heat transfer for flow boiling of water in vertical rod bundles. In: Paper B4.9, IVth International Heat Transfer Conference, Paris-Versailles.

Owens, W.S., 1961. Two-phase pressure gradient. Int. Dev. Heat Transfer, Part II. ASME.

Pioro, I.L., 2016. In: Pioro, I.L. (Ed.), Handbook of generation IV nuclear reactors, 103. Woodhead Publishing Series in Energy: Elsevier, UK.

Pioro, I.L., Duffey, R.B., 2007. Heat transfer and hydraulic resistance at supercritical pressures in power engineering applications. ASME press, Three Park Avenue, New York, NY 10016, USA.

Rehme, K., 1968. Systematische experimentelle Untersuchung der Abhängigkeit des Druckverlustes von der geometrischen Anordnungfürlängs durch strömte Stabbündel mit Spiraldraht-Abstandshaltern. KfK, Rep. 4/68-16.

Rehme, K., 1969. Druckverlust in Stabbündeln mit Spiraldraht-Abstandshaltern. Forsh. Ing.-Wes 35 (Nr.4).

Rehme, K., 1973. Pressure drop correlations for fuel element spacers. Nucl. Technol. 17, 15–23.

Rehme, K., 1977. Pressure drop of spacer grids in smooth and roughened rod bundles. Nucl. Technol. 33, 313–317.

Rouhani, S.Z., 1969. Subcooled void fraction. AB Atomenergi, Sweden, Rept. AWE-RTV-841.

Saha, P., Zuber, N., 1974. Point of net vapour generation and void fraction in subcooled boiling Paper B4.7. In: Proc. 5th Int. Heat Transfer Conf., pp. 175–179.

Selander, W.N., 1978. Explicit formulas for the computation of friction factors in turbulent pipe flow. AECL-6354, Atomic Energy of Canada Limited., Chalk River Nuclear Laboratories, Chalk River, Ontario KOJ IJO, November 1978.

Serrano-Lopez, R., Fradera, J., Cuesta-Lopez, S., 2013. Molten salts database for energy applications. Chem. Eng. Processing: Process Intensification 73, 87–102.

Sieder, E.N., Tate, G.E., 1936. Heat transfer and pressure drop of liquids in tubes. Ind. Eng. Chem. 28, 1429–1435.

Sekoguchi, K., Saito, Y., Honda, T., 1970. JSME Preprint No. 700-7, 83.

Shah, M.M., 1982. Chart correlation for saturated boiling heat transfer: equations and further study. ASHRAE Trans. 88, 185–196.

Snoek, C.W., Ahmad, S.Y., 1983. A method of predicting pressure profiles in horizontal 37-element clusters. AECL-8065, Chalk River, Ontario.

Snoek, C.W., Leung, L.K.H., 1989. A model for predicting diabatic pressure drops in multielement fuel channels. Nucl. Eng. Design 110, 299–312.

Sobolev, V., 2010. Database of thermophysical properties of liquid metal coolants for GEN-IV, SCK. CEN-BLG-1069, SCK. CEN, Boeretang 200, 2400 Mol Belgium.

Song, J.H., Ishii, M., 2001. On the stability of a one-dimensional two-fluid model. Nucl. Eng. Design 204, 101–115.

Swapnalee, B.T., Vijayan, P.K., 2011. A generalized flow equation for single-phase natural circulation loops obeying multiple friction laws. Int. J. Heat Mass Transfer 54, 2618–2629.

Swapnalee, B.T., Vijayan, P.K., Sharma, M., Pilkhwal, D.S., 2012. Steady state flow and static instability of supercritical natural circulation loops. Nucl. Eng. Design 245, 99–112.

Tarasova, N.V., et al., 1966. Pressure drop of boiling subcooled water and steam mixture flowing in heated channels. In: Proceedings of 3rd International Heat Transfer Conference, vol. IV, pp. 178–183.

Thirumaleshwar, M., 2006. Fundamentals of Heat and Mass Transfer. Pearson Educ, pp. 454–455.

Thom, J.R.S., 1964. Prediction of pressure drop during forced circulation boiling of water. Int. J. Heat Mass Transfer 7, 709–724.

Vijayan, P.K., Prabhakar, B., Venkat Raj, V., 1981. Experimental measurement of pressure drop in diabatic two-phase flow and comparison of predictions of existing correlations with the experimental data. H-13. In: 6th National Heat and Mass Transfer Conference, IIT Madras, India.

Vijayan, P.K., Austregesilo, G.S., Teschendorf, V., 1995. Simulation of the unstable oscillatory behaviour of single-phase natural circulation with repetitive flow reversals in a rectangular loop using the computer code ATHLET. Nucl. Eng. Design 155 (1995), 623–641.

Vijayan, P.K., Pilkhwal, D.S., Saha, D.S., Venkat Raj, V., 1999. Experimental studies on the pressure drop across the various components of a PHWR fuel channel. Exp. Therm. Fluid Sci. 20, 34–44.

Vijayan, P.K., Patil, A.P., Pilkhwal, D.S., Saha, D., Venkat Raj, V., 2000. An assessment of pressured drop and void fraction correlations with data from two-phase natural circulation loops. Heat Mass Transfer 36, 541–548.

Von Karman, T., 1930. Nach. Ges. Wiss. Gottingen, Fachgruppe I, 5, pp. 58–76.

Wang, S., Yuan, L., Leung, L., 2010. Assessment of supercritical heat transfer correlations against AECL database for tubes. In: Proc. 2nd Canada-China Joint Workshop on supercritical water-cooled reactors, Toronto, Canada, April 25–28.

Weisman, J., Choe, W.G., 1976. Methods for calculation of pressure drop in concurrent gas liquid flow. In: Proc. Two-phase Flow and Heat Transfer Symp. Workshop, Fort Lauderdale, Two-Phase Transport and Reactor Safety, vol. 1.

Yagi, S., 1954. Chem. Eng. (Japan) 18, 2.

Yang, S.K., Khartabil, H.F., 2005. Normal and deteriorated heat transfer correlations for supercritical fluids. In: Transactions, ANS Meeting, Washington, DC, 95, November, pp. 635–637.

Yildirim, G., 2009. Computer-based analysis of explicit approximations to the implicit Colebrook-White equation in turbulent flow friction factor calculation. Adv. Eng. Software 40, 1183–1190.

Zhou, J., Podowski, M.Z., 2001. Modeling and analysis of hydrodynamic instabilities in two-phase flow using two-fluid model. Nucl. Eng. Design 204, 129–142.

Further reading

Blasius, P.R.H., 1913. Das Aehnlichkeitsgesetz bei Reibungsvorgangen in Flussigkeiten. Forschungsheft 131, 1–41.

Dittus, F.W., Boelter, L.M.K., 1930. University California Publs. Eng. 2, 443.

Drew, T.B., Koo, E.C., McAdams, 1932. Trans. AIChE, 28:56.

Khare, R., Vijayan, P.K., Saha, D., Venkat Raj, V. 1997. Assessment of theoretical flow pattern maps for vertical upward two-phase flow. BARC/1997/E010, 1997.

Pioro, I.L., Duffey, R.B., 2005. Experimental Heat transfer to supercritical water flowing inside channels (survey). Nucl. Eng. Design 235, 2407–2420.

Rehme, K., Trippe, G., 1980. Pressure drop and velocity distribution in rod bundles with spacer grids. Nucl. Eng. Design 62, 349–359.

Xu, F., 2004. Study on flow and heat transfer characteristics of water in tubes at supercritical pressures. Master Degree Thesis, Xi'an, China (in Chinese).